Phenomenology of scalar leptoquarks at the LHC in explaining the radiative neutrino masses, muon $g-2$, and lepton flavor violating observables

Snehashis Parashar,[1,*] Anirban Karan,[2,†] Avnish,[3,4,‡] Priyotosh Bandyopadhyay,[1,§] and Kirtiman Ghosh[3,4,‖]

[1]*Indian Institute of Technology Hyderabad, Kandi, Sangareddy 502284, Telangana, India*
[2]*Instituto de Física Corpuscular (CSIC—Universitat de València), Apartado Correus 22085, E-46071 València, Spain*
[3]*Institute of Physics, Bhubaneswar, Odisha 751005, India*
[4]*Homi Bhabha National Institute, Training School Complex, Anushakti Nagar, Mumbai 400094, India*

(Received 26 September 2022; accepted 14 November 2022; published 30 November 2022; corrected 20 January 2023)

We study the phenomenology of a particular leptoquark extension of the Standard Model (SM), namely the doublet-singlet scalar leptoquark extension of the SM (DSL-SM). Besides generating Majorana mass for neutrinos, these leptoquarks contribute to muon and electron $(g-2)$ and various lepton flavor violating processes. Collider signatures of the benchmark points (BPs), consistent with the neutrino oscillation data, anomalous muon/electron magnetic moments, experimental bounds on the charged lepton flavor violation observables, etc., are studied at the LHC/FCC with center-of-mass energies of 14, 27 and 100 TeV. While the two $-1/3$ charged colored scalars from the singlet and the doublet leptoquark mix with each other, the charge $2/3$ colored scalar from the doublet leptoquark remains pure. With a near-degenerate mass spectrum, the pure and mixed leptoquark states are shown to be distinguishable from multiple final states, while discerning between the two mixed states remains very challenging.

DOI: 10.1103/PhysRevD.106.095040

I. INTRODUCTION

Though the Standard Model (SM) provides a beautiful theoretical explanation of the nongravitational interaction of the elementary particles in terms of $SU(3)_C \otimes SU(2)_L \otimes U(1)_Y$ gauge group, there is ample evidence that it is not a complete theory. Neutrino oscillation indicating the nonzero masses of neutrinos and flavor mixing of leptons is one of such phenomena advocating the incompleteness of the SM which predicts massless neutrinos without any flavor mixing. While the simplest way to generate neutrino masses is to add right-handed neutrino fields to the SM particle content, it is hard to explain their extreme smallness. Such a small mass could be understood if neutrinos are Majorana particles and Majorana masses for neutrinos are generated from higher dimensional operators who violate the lepton number by two units. The most studied example of such an operator is the dimension-5 Weinberg operator [1]: $\mathcal{O}_5 = \frac{c_{\alpha\beta}}{\Lambda}(\overline{L^C_{\alpha L}}\tilde{H}^*)(\tilde{H}^\dagger L_{\beta L})$, where α, β are the generation indices, $L_L = (\nu_L, l_L)^T$ is the left-handed lepton doublet of the SM, $H = (H^+, H^0)^T$ is the Higgs doublet and $\tilde{H} = i\sigma_2 H^*$. Λ is the scale of new physics, and $c_{\alpha\beta}$ is a model-dependent coefficient. The Weinberg operator gives rise to Majorana masses (suppressed by Λ) for the neutrinos after electroweak symmetry breaking (EWSB). At tree level, there are only three ways to generate the Weinberg operator, namely, the type-I [2–5], the type-II [6–14] and the type-III [15–17] seesaw mechanisms. In the framework of tree-level seesaw models, the smallness of neutrino masses (m_ν) is explained via new physics at a very high scale of Λ. Though the seesaw models are naturally motivated to have very high scale masses to explain the tinyness of the neutrino masses, if balanced with appropriate Yukawa couplings, nothing precludes them from having mass at the TeV scale and hence testable at the collider experiments. Note that the simplest TeV scale seesaw models are tightly constrained from the stringent cosmological upper bound of $\lesssim 0.09$ eV on the total mass $(\sum m_\nu)$ of light neutrinos [18], charged lepton flavor violating (CLFV) observables, electroweak (EW) precision observables, vacuum stability and perturbativity of the scalar potential (in the context of type-II seesaw only) [19–21], and collider experiments. However, one can construct an alternative class of models in which $\mathcal{O}_5$ is forbidden at the tree level, and neutrino masses are

*ph20resch11006@iith.ac.in
†kanirban@ific.uv.es
‡avnish@iopb.res.in
§bpriyo@phy.iith.ac.in
‖kirtiman.ghosh@iopb.res.in

generated radiatively [22–34] or from a tree-level effective operator [35–40] with mass dimension $d > 5$. The additional suppression[1] to the neutrino masses arises from the loop integrals (in the case of the former) or higher powers of Λ in the denominator (in the case of the latter), brings down the new physics scale Λ to TeV scale and, hence, makes these models testable at the LHC.

Apart from neutrino mass generation, the anomalous magnetic moment of muon is another long-standing puzzle in particle physics. The combined result from Fermi National Accelerator Laboratory [41] and Brookhaven National Laboratory [42] suggests a 4.2σ deviation in the measurement of $a_\mu (\equiv \frac{g_\mu}{2} - 1)$ from its theoretical estimate under SM[2] [43–52]: $\Delta a_\mu = a_\mu^{\mathrm{Ex}} - a_\mu^{\mathrm{SM}} = (2.51 \pm 0.59) \times 10^{-9}$. Similar anomaly exists for electron $(g-2)$ also. But, while the experiment with cesium shows $\Delta a_e^{Cs} = a_e^{Ex}(Cs) - a_e^{\mathrm{SM}} = (-8.8 \pm 3.6) \times 10^{-13}$ [53], the same with rubidium suggests $\Delta a_e^{Rb} = a_e^{Ex}(Rb) - a_e^{\mathrm{SM}} = (4.8 \pm 3.0) \times 10^{-13}$ [54]. Though the expectation values of Δa_e in the two experiments are large and opposite in sign, the significances of the measurements are reduced due to large experimental error bars.

It is important to note that the current experimental data (from neutrino oscillation as well as scattering experiments) is inconclusive in determining the actual mechanism of neutrino mass generation. However, it is clear that the massive neutrinos and anomalous magnetic moment of the charged leptons are both experimentally facts, and hence, should be incorporated into the extensions of the SM. It would be particularly exciting if a single mechanism resolves two of these important outstanding puzzles in particle physics. It has been shown in the literature [55,56] that the minimal tree-level seesaw models are not very efficient in incorporating these $(g-2)$ anomalies. This necessitates searching for some other mechanism to provide a combined explanation for neutrino mass generation as well as muon $(g-2)$. The SM particle spectrum extended by TeV scale leptoquarks could be a possible answer to this puzzle. However, attempts to construct a unified theory that explains nonzero neutrino masses/mixings and anomalous magnetic moments of the SM charged leptons suffer, typically, from roadblocks in the form of unacceptable phenomenological consequences such as large contributions to the SM charged lepton flavor violating processes. In particular, any ultraviolet complete theory designed to explain the anomalous magnetic moments would necessarily contain additional fields. If we want these fields to play a role in generating neutrino masses and mixings, there is always the danger of enhancing the SM charged lepton flavor-violating processes such as $\mu \to e\gamma$, $\mu \to 3e$, μ-e conversion in nuclei, etc. which are tightly constrained from different charged lepton flavor violation experiments. In other words, the introduction of new fields and their interactions cannot be arbitrary, for not only must low-energy observables remain consistent with measurements, but the failure of collider experiments to observe such particles must be explained. Note that models comprising doublet-singlet or doublet-triplet leptoquarks [57–65] with Yukawa interactions involving the SM lepton, quark multiplets, and the leptoquarks are known to generate Majorana masses for the neutrinos at the one-loop level and also contribute to the $g-2$ of the SM charged leptons. A comprehensive study of such a framework in the context of neutrino oscillation data, $g-2$ anomalies, bounds on the CLFV observables, and collider experiments is missing in the literature. This article intends to fill this gap.

Leptoquark models where the SM field content is enlarged by introducing colored scalars (spin-0) or vector (spin-1) fields have been there in literature for quite a few decades [66,67]. They emerge naturally in higher gauge theories unifying matters [66–77]. Being charged under the $SU(3)_C$, the Yukawa interactions of the scalar leptoquarks simultaneously involve a quark and a lepton and hence provide an elegant explanation for the recent observation of the lepton flavor nonuniversality in the B-meson decays. The prospect of leptoquark models in resolving various flavor anomalies along with neutrino mass generation and muon $(g-2)$ makes them discussable in recent times [78–103]. The phenomenology of leptoquark models has been studied in literature [104–139], especially in the context of the Large Hadron Collider (LHC) experiment. For example, leptoquarks have been searched experimentally at various colliders including the LHC over the past three decades [140–153]; however, their existence is yet to be confirmed. Discerning features of different scalar and vector leptoquarks at electron-photon [154], electron-proton [155] and proton-proton [134,156,157] colliders have been investigated relying dominantly on the angular distribution. Constraints from Planck scale stability and perturbativity on different scalar leptoquarks have also been studied [158,159].

In this work, the field content of the SM is extended to include the following pair of scalar leptoquarks [57] nontrivially charged under the SM gauge symmetry $[\mathbf{SU(3)_C}, \mathbf{SU(2)_L}, \mathbf{U(1)_Y}]$: S_1 $(\bar{\mathbf{3}}, \mathbf{1}, 1/3)$ and $\tilde{R}_2$ $(\mathbf{3}, \mathbf{2}, 1/6)$ [59,60,63,65,160–163].[3] The most general scalar potential and Yukawa interactions involving the SM fields and the

[1]Note that the typical scale of a new physics, where neutrino mass is generated via a d-dimensional operator at n-loop level, can be estimated from the following neutrino mass formula: $m_\nu \propto (\frac{1}{16\pi^2})^n \times \frac{\mathrm{VEV}^{d-3}}{\Lambda^{d-4}}$.

[2]It is worth mentioning that the combined experimental result is compared against the data-driven SM prediction from [43] which leads to the 4.2σ deviation, not taking into account the lattice QCD prediction from [44], which is in fact closer to the experimental average.

[3]We also restrict ourselves to one generation of leptoquarks with off-diagonal Yukawa coupling, to avoid the constraints from perturbative unitarity [159].

leptoquarks, S_1 and $\tilde{R}_2$, violate the lepton number conservation and result in nonzero Majorana masses for the neutrinos at the one-loop level. In other words, one needs to consider both S_1 and $\tilde{R}_2$ simultaneously in the model to successfully generate the $d = 5$ Weinberg operator for neutrino mass at one loop [22]. Both the singlet and doublet leptoquark in this model contributes to the charged lepton $g-2$ and CLFV processes. We studied the possibility of simultaneously explaining neutrino oscillation data and muon anomalous magnetic moment in the framework of this model subjected to the experimental constraints from the CLFV experiments. We obtain benchmark points that are consistent with all the observational constraints, such as neutrino oscillation data, muon $(g-2)$ and lepton flavor violating decays, etc. The second part of the article is dedicated to the collider signatures of those benchmark points at the LHC experiment. The particle spectrum of this model includes two exotic colored scalars (denoted as mixed states) with electric charge $\frac{1}{3}$ resulting from the mixing of $\frac{1}{3}$ components of the singlet and doublet leptoquarks. Another exotic colored scalar (denoted as the pure state) with electric charge $\frac{2}{3}$ results from the doublet leptoquark. While this particular leptoquark combination has been extensively studied in literature in the context of various bounds and anomalies, to our knowledge, a detailed study of final states resulting from different choices of the Yukawa couplings, at the current and future iterations of the LHC, has not been explored for this model. We provide a thorough study of the production, decay, and resulting collider signatures of these exotic scalars for a carefully chosen set of benchmark points at the current LHC, as well as the future high energy (HE)/high luminosity (HL)-LHC [164,165], and the future circular collider (FCC) [166]. Along with the discovery prospect of the model at the LHC/FCC, our analysis on multiple final states that can help in distinguishing between the physical mass eigenstates of the leptoquarks in this model is presented, for a near-degenerate mass spectrum. Additionally, we suggest a method of probing the leptoquark mixing angle at a future high-energy and high-precision hadron collider, via asymmetric pair production with t-channel $W^{\pm}$-boson exchange.

This article is organized as follows: in the next section (Sec. II), we introduced the model with a discussion on neutrino mass generation, anomalous magnetic moments of charged leptons and leptoquark contributions to the CLFV processes. In Sec. III, the choice of our benchmark points from neutrino oscillation data, $(g-2)$ and CLFV processes is motivated. The subsequent section (Sec. IV) deals with a collider probe of the model at the LHC/FCC through pair production for the chosen benchmark points. In Sec. V, we discuss the distinguishing signatures of the pure and mixed leptoquark states from pair production. The next section (Sec. VI) is dedicated to the challenges in differentiating between the two mixed leptoquark states in the context of our benchmark points, complemented with a discussion on probing the leptoquark mixing angle. Finally, we summarize our results in Sec. VII.

II. THE MODEL

In addition to all the SM particles, the model includes a scalar $SU(2)_L$ doublet leptoquark $\tilde{R}_2(\mathbf{3},\mathbf{2},1/6) = (\tilde{R}_2^{2/3}, \tilde{R}_2^{-1/3})^T$ and a singlet leptoquark $S_1(\bar{\mathbf{3}},\mathbf{1},1/3)$ [65]. The relevant part of the Lagrangian involving the leptoquarks is given as

$$\begin{aligned}-\mathcal{L} \supset\ & [\mathcal{Y}_1^L \bar{\boldsymbol{Q}}_L^c S_1 (i\sigma_2) \boldsymbol{L}_L + \mathcal{Y}_1^R \bar{u}_R^c S_1 \ell_R + \mathcal{Y}_2 \bar{d}_R \tilde{R}_2^T (i\sigma_2) \boldsymbol{L}_L \\ & + \kappa H^\dagger \tilde{R}_2 S_1 + \text{H.c.}] + m_1^2 (S_1^\dagger S_1) + m_2^2 (\tilde{R}_2^\dagger \tilde{R}_2) \\ & + \alpha_1 (H^\dagger H)(S_1^\dagger S_1) + \alpha_2 (H^\dagger H)(\tilde{R}_2^\dagger \tilde{R}_2) \\ & + \alpha_2' (H^\dagger \tilde{R}_2)(\tilde{R}_2^\dagger H), \end{aligned} \tag{2.1}$$

where, $\boldsymbol{Q}_L(\mathbf{3},\mathbf{2},1/6)$ and $\boldsymbol{L}_L(\mathbf{1},\mathbf{2},-1/2)$ represent the left-handed quark and lepton doublets with three generations, $d_R(\mathbf{3},\mathbf{1},-1/3)$ indicates the right-handed singlet for down-type quark with all the three generations and $H(\mathbf{1},\mathbf{2},1/2)$ is the SM Higgs doublet. Here, σ_2 denotes the second Pauli matrix, the superscripts "c" and "T" signify charge conjugation and transpose in $SU(2)_L$ space, respectively. $\mathcal{Y}_1^{L,R}$ and $\mathcal{Y}_2$ are 3×3 complex matrices describing the Yukawa interactions of the leptoquarks S_1 and $\tilde{R}_2$, respectively with different quarks and leptons. The terms m_1 and m_2 are mass terms for the singlet and the doublet leptoquarks, respectively. α_1, α_2 and α_2' are real dimensionless couplings describing the strength of quartic interaction between the leptoquarks and the SM Higgs doublet, whereas the trilinear coupling κ is in general complex with mass dimension one and plays a crucial role in the phenomenology of this model. Note that in Eq. (2.1) simultaneous presence of the Yukawa couplings $\mathcal{Y}_1^L$ and $\mathcal{Y}_2$ in association with the trilinear scalar coupling κ violates lepton number in the model. However, we keep only those terms in the Lagrangian that preserve baryon number (B), which leads to the absence of the diquark coupling terms with S_1, as well as the quartic term of the form $S_1^2 \tilde{R}_2^\dagger H$. The presence of such terms can lead to fast proton decay [167], and naturally we wish to avoid that. Assigning $B = -1/3$ to S_1 and $B = +1/3$ to $\tilde{R}_2$ ensures the absence of these terms in the Lagrangian. Moreover, the trilinear coupling results into mixing among the singlet (S_1) and electromagnetic charge $\frac{1}{3}$ component of the doublet ($\tilde{R}_2{}^{1/3}$) leptoquark after the EWSB. The mass matrix involving S_1 and $\tilde{R}_2{}^{1/3}$ is given by

$$\mathcal{M}^2_{LQ} = \begin{pmatrix} m^2(S_1) & \frac{\kappa v}{\sqrt{2}} \\ \frac{\kappa v}{\sqrt{2}} & m^2(\tilde{R}_2^{1/3}) \end{pmatrix}, \tag{2.2}$$

where v is the vacuum expectation value (VEV) of the SM Higgs doublet, $m^2(S_1) = m_1^2 + \frac{1}{2}\alpha_1 v^2$ and $m^2(\tilde{R}_2^{1/3}) = m_2^2 + \frac{1}{2}(\alpha_2 + \alpha_2')v^2$. The physical electromagnetic (EM) charge $\frac{1}{3}$ scalars ($X_1^{1/3}$ and $X_2^{1/3}$) are obtained by diagonalizing the mass matrix in Eq. (2.2) and given by

$$\begin{aligned} X_1^{1/3} &= \cos\theta_{LQ} S_1^{1/3} + \sin\theta_{LQ}\tilde{R}_2^{1/3}, \\ X_2^{1/3} &= -\sin\theta_{LQ} S_1^{1/3} + \cos\theta_{LQ}\tilde{R}_2^{1/3}, \end{aligned} \tag{2.3}$$

where θ_{LQ} is the mixing angle given by

$$\tan 2\theta_{LQ} = \frac{-\sqrt{2}\kappa v}{m^2(S_1) - m^2(\tilde{R}_2^{1/3})}, \tag{2.4}$$

and the mass eigenvalues of the mixed leptoquark eigenstates are obtained as

$$\begin{aligned} M^2_{1,2} = \frac{1}{2}\Big[& m^2(S_1) + m^2(\tilde{R}_2^{1/3}) \\ & \mp \sqrt{\{m^2(S_1) - m^2(\tilde{R}_2^{1/3})\}^2 + 2v^2\kappa^2}\Big], \end{aligned} \tag{2.5}$$

whereas the mass of the pure doublet leptoquark with EM charge $\frac{2}{3}$ is given by

$$m^2(\tilde{R}_2{}^{2/3}) = m_2^2 + \frac{1}{2}\alpha_2 v^2. \tag{2.6}$$

A. Loop induced neutrino masses, CLFV, and $(g-2)$

In the framework of this model, Majorana mass of the light neutrinos is generated at the one-loop level via the Feynman diagram depicted in Fig. 1, where the simultaneous presence of the Yukawa couplings, $\mathcal{Y}_1^L$, $\mathcal{Y}_2$, and scalar trilinear coupling κ leads to the lepton number violation. In the absence of any of the aforementioned couplings, this mass term vanishes. The light neutrino mass matrix from this diagram is obtained as [60][4]

$$M_\nu \simeq \frac{3\sin 2\theta_{LQ}}{32\pi^2}\ln\left(\frac{M_1^2}{M_2^2}\right)[\mathcal{Y}_1^L m_d \mathcal{Y}_2^T + \mathcal{Y}_2 m_d (\mathcal{Y}_1^L)^T], \tag{2.7}$$

where, m_d is the diagonal mass matrix for down-type quarks. In the above equation, it has been assumed that the leptoquarks are very heavy compared to the mass of all the down-type quarks.

[4]Here, Yukawa couplings of leptoquarks are considered to be real.

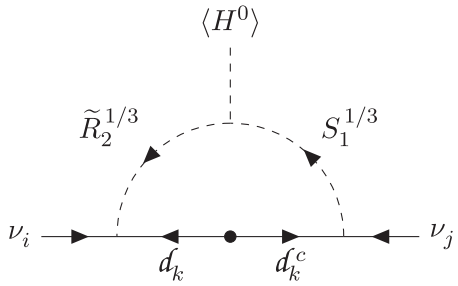

FIG. 1. One-loop diagrams for generation of neutrino mass matrix through leptoquarks with (i, j, k) being generation indices.

In this model, leptoquarks also contribute to CLFV processes like $l_i \to l_j\gamma$ at one-loop order, as shown in Fig. 2. In this work, we have implemented the model in SARAH [168] to generate model files for SPheno [169,170] and MadGraph5 [171] to numerically compute the mass spectrum, decays, different low energy observables including the CLFV processes, charged lepton anomalous magnetic moments, and collider signatures, respectively. However, for the sake of completeness and understanding about the dependence of CLFV processes and charged lepton anomalous magnetic moments on the Yukawa couplings, approximate analytical expressions for the $\mathcal{B}(l_i \to l_j\gamma)$ and Δa_l are summarized in the following.

In the framework of this model, the branching fraction for the ith charged lepton flavor violating decay into jth lepton and a photon, $\mathcal{B}(l_i \to l_j\gamma)$ can be expressed as [65]

$$\begin{aligned} \mathcal{B}(l_i \to l_j\gamma) = \frac{e^2(m_i^2 - m_j^2)^3}{4096\pi^5 m_i^3 \Gamma_i}[& |\mathcal{A}_L^{X_1} + \mathcal{A}_L^{X_2} + \mathcal{A}_L^{\tilde{R}_2^{2/3}}|^2 \\ & + |\mathcal{A}_R^{X_1} + \mathcal{A}_R^{X_2} + \mathcal{A}_R^{\tilde{R}_2^{2/3}}|^2], \end{aligned} \tag{2.8}$$

where $m_{i,j}$ are the masses of the charged leptons with flavor (i, j) and Γ_i the total decay width of ith lepton. Now, the loop functions $\mathcal{A}$ are given by

$$\begin{aligned} \mathcal{A}_L^{X_{1,2}} = \frac{\mathcal{C}_{1,2}^2}{4M_1^2}\Bigg[& 2(\tilde{\mathcal{Y}}_1^L)_{ki}(m_u^{kk})(\mathcal{Y}_1^R)_{kj}\mathcal{F}\left\{\frac{(m_u^{kk})^2}{M_{1,2}^2}\right\} \\ & - \left\{m_j(\tilde{\mathcal{Y}}_1^L)_{ki}(\tilde{\mathcal{Y}}_1^L)_{kj} + m_i(\mathcal{Y}_1^R)_{ki}(\mathcal{Y}_1^R)_{kj}\right\} \\ & \times \mathcal{G}\left\{\frac{(m_u^{kk})^2}{M_{1,2}^2}\right\}\Bigg], \end{aligned} \tag{2.9}$$

$$\begin{aligned} \mathcal{A}_R^{X_{1,2}} = \frac{\mathcal{C}_{1,2}^2}{4M_1^2}\Bigg[& 2(\mathcal{Y}_1^R)_{ki}(m_u^{kk})(\tilde{\mathcal{Y}}_1^L)_{kj}\mathcal{F}\left\{\frac{(m_u^{kk})^2}{M_{1,2}^2}\right\} \\ & - \{m_i(\tilde{\mathcal{Y}}_1^L)_{ki}(\tilde{\mathcal{Y}}_1^L)_{kj} + m_j(\mathcal{Y}_1^R)_{ki}(\mathcal{Y}_1^R)_{kj}\} \\ & \times \mathcal{G}\left\{\frac{(m_u^{kk})^2}{M_{1,2}^2}\right\}\Bigg], \end{aligned} \tag{2.10}$$

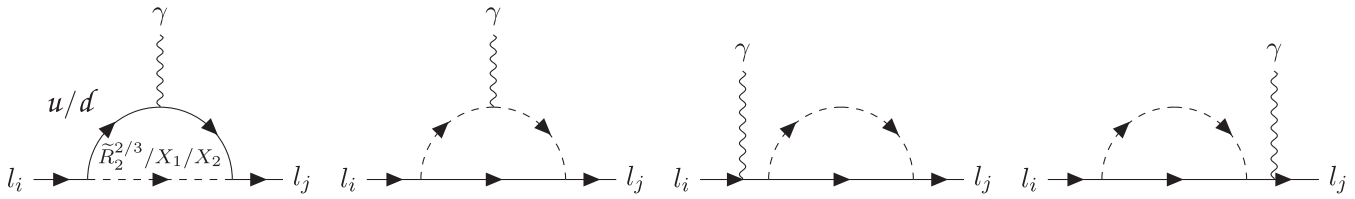

FIG. 2. One-loop diagrams contributing to $l_i \to l_j\gamma$. The same diagrams will contribute to $g-2$ of muon and electron for $i=j$.

$$\mathcal{A}_L^{\tilde{R}_2^{2/3}} = -\frac{m_j}{4m^2(\tilde{R}_2^{2/3})}(\mathcal{Y}_2)_{ki}(\mathcal{Y}_2)_{kj}\mathcal{I}\left\{\frac{(m_d^{kk})^2}{m^2(\tilde{R}_2^{2/3})}\right\},$$
$$\mathcal{A}_L^{\tilde{R}_2^{2/3}} = -\frac{m_i}{4m^2(\tilde{R}_2^{2/3})}(\mathcal{Y}_2)_{ki}(\mathcal{Y}_2)_{kj}\mathcal{I}\left\{\frac{(m_d^{kk})^2}{m^2(\tilde{R}_2^{2/3})}\right\}, \quad (2.11)$$

where $\tilde{\mathcal{Y}}_1^L = V\mathcal{Y}_1^L$ (V being the usual Cabibbo-Kobayashi-Maskawa (CKM) matrix), $\mathcal{C}_1 = \cos\theta_{LQ}$, $\mathcal{C}_2 = \sin\theta_{LQ}$ along with

$$\mathcal{F}(x) = \frac{7-8x+x^2+2(2+x)\ln x}{(1-x)^3},$$
$$\mathcal{G}(x) = \frac{1+4x-5x^2+2x(2+x)\ln x}{(1-x)^4}, \quad (2.12)$$

$$\mathcal{I}(x) = \frac{x[5-4x-x^2+2(1+2x)\ln x]}{(1-x)^4}. \quad (2.13)$$

It is important to mention here that we use the convention of rotating the flavor eigenstates of up-type quarks by the CKM matrix to obtain their mass eigenstates.[5] Therefore, the left-handed Yukawa coupling $\mathcal{Y}_1^L$ changes to $\tilde{\mathcal{Y}}_1^L$ in the square of amplitude while considering the interaction of an up-type quark with a charged lepton through leptoquark S_1 (i.e. in the mass basis through the singlet component of $X_{1,2}^{-1/3}$), while the rest of the couplings between quarks and leptons through leptoquarks remain unaltered.

The additional contribution, resulting from the leptoquarks in the loop, to the jth charged lepton magnetic moment can be expressed in the following way:

$$\Delta a_j = \Delta a_j^{X_1} + \Delta a_j^{X_2} + \Delta a_j^{\tilde{R}_2^{2/3}}, \quad (2.14)$$

$$\Delta a_j^{X_{1,2}} = -\frac{\mathcal{C}_{1,2}^2 m_j}{32\pi^2 M_1^2}\left[2(m_u^{kk})(\tilde{\mathcal{Y}}_1^L)_{kj}(\mathcal{Y}_1^R)_{kj}\mathcal{F}\left\{\frac{(m_u^{kk})^2}{M_{1,2}^2}\right\}\right.$$
$$\left. - m_j\{|(\tilde{\mathcal{Y}}_1^L)_{kj}|^2 + |(\mathcal{Y}_1^R)_{kj}|^2\}\mathcal{G}\left\{\frac{(m_u^{kk})^2}{M_{1,2}^2}\right\}\right], \quad (2.15)$$

$$\Delta a_j^{\tilde{R}_2^{2/3}} = \frac{m_j^2|(\mathcal{Y}_2)_{kj}|^2}{32\pi^2 m^2(\tilde{R}_2^{2/3})}\mathcal{I}\left\{\frac{(m_d^{kk})^2}{m^2(\tilde{R}_2^{2/3})}\right\}, \quad (2.16)$$

[5]For the choice of our benchmark points, we have used SPheno which uses the same convention.

with all the relevant functions defined above. One can argue from the above expressions that for TeV-scale leptoquark masses, the contribution from $\tilde{R}_2^{+2/3}$ in explaining the experimental excess of muon $(g-2)$ is negligible compared to $X_{1,2}^{-1/3}$, and assuming no mixing, S_1 alone can explain the excess. However, we inevitably require both of these leptoquarks in the model to generate the Majorana neutrino mass as discussed, and hence we consider the muon $(g-2)$ contribution from both $\tilde{R}_2^{+2/3}$ and $X_{1,2}^{-1/3}$, for the sake of completeness. The muon-electron conversion rate with the presence different nuclei for generic leptoquark model has been discussed using the effective field theory approach in Ref. [136].

III. BENCHMARK POINTS

The primary goal of this work is to probe the model at the LHC/FCC for the particular set of model parameters, which are not only consistent with the neutrino mass and oscillation data, but also satisfy the current experimental values of electron and muon $g-2$, while respecting the upper bounds on CLFV decays of charged leptons. Following the brief introduction of the model including radiative neutrino mass generation, CLFV processes and $g-2$, we are now equipped enough to search for benchmark points on which we will perform the collider study.

We diagonalize the neutrino mass matrix of Eq. (2.7) to obtain the Yukawa couplings $\mathcal{Y}_1^L$ and $\mathcal{Y}_2$ which are consistent with the neutrino mass sum and mass-squared difference limits. Then, we utilize SPheno [169,170] version 4.0.4 to find out which set of such couplings can satisfy the $g-2$ data simultaneously with the neutrino mass data, with adequate choices of entries in $\mathcal{Y}_1^R$. Then, with the help of SPheno, the CLFV observables are obtained for such couplings, while keeping them consistent with the neutrino oscillation parameters as well. In the following, we list three benchmark points (BPs), each with different phenomenological aspect. The parameters of the scalar potential are kept fixed across the three BPs as noted in

TABLE I. Parameters except Yukawa couplings for all the BPs (at 5 GeV renormalization scale of SPheno).

Parameters	m_1	m_2	α_1	α_2	α_2'	κ
Values	1.5 TeV	1.5 TeV	0.2	0.2	0.2	50 GeV

Table I. The masses of the leptoquarks m_1 and m_2 are considered in accordance with the LHC data at the 2σ level [172–174]. For this set of parameters in Table I, we obtain $\theta_{LQ} = -0.618$ radians. This leads to X_1 containing ~66.5% of S_1 and ~33.5% of $\tilde{R}_2^{1/3}$ while for X_2 these proportions get reversed.

It is worth mentioning here that generic studies of the parameter space of this model exist in contemporary literature [65,160], taking into account different sets of bounds alongside the neutrino mass generation. Reference [160], for example, presents a parameter scan for the $\tilde{R}_2 + S_1$ combination considering not only the muon $g-2$ and CLFV bounds, but also the various B-decay anomalies and the latest CDF-II measurement of the $W^{\pm}$-mass [175], with complex Yukawa couplings. In our work however, the collider searches for these leptoquarks are given prime importance, which requires adherence to a set of benchmark scenarios. We wish to perform a detailed and comparative study of multiple final states at the LHC/FCC, and hence we have strategically chosen our BPs in such a way that the Yukawa couplings follow three different regimes of relative strength, in an attempt to draw a more comprehensive picture of the parameter space and their respective phenomenology. For our first BP, the entries of the $\mathcal{Y}_2$ are taken to be very tiny in comparison to those of $\mathcal{Y}_1^L$, as prescribed in [60]. In the second regime, i.e. BP2, two entries of $\mathcal{Y}_2$ are chosen in the same order of magnitude as those of $\mathcal{Y}_1^L$. Lastly, in the third benchmark scenario, $\mathcal{Y}_2$ contains an element that is larger than any of those in $\mathcal{Y}_1^L$, leading to more impact of the leptoquark mixing in the decay branching ratios. All these BPs are fine-tuned to respect the indirect bounds from neutrino oscillation data and CLFV decays, and if one wishes to perform a generic collider study over a large parameter space, one can certainly extrapolate these three regimes by varying the Yukawa couplings around the chosen BPs, which may lead to changes in the values corresponding to the indirect bounds.

In the subsections that follow, we will discuss the choice of our benchmark points from the perspective of each of the sets of bounds that we prioritize. The extremely sensitive nature of the bounds from neutrino mass and oscillation, anomalous magnetic moment, and other CLFV observables means we require very high precision on the Yukawa couplings to satisfy all of them simultaneously. However, from a collider perspective, it is not possible to probe Yukawa couplings up to such accuracy. Therefore, we start off with the neutrino masses as our first priority, and choose the couplings up to the least decimal point with which these sub-eV masses are satisfied within the mass sum and mass squared difference limits. The next immediate priority is given to the muon and electron $g-2$ measurements. After that, the required fine-tuning to satisfy the neutrino oscillation data and the CLFV bounds will be discussed.

A. Choice of Yukawa couplings

As discussed previously, the couplings stated here are kept up to the lowest possible precision that are in agreement with the resultant neutrino mass eigenvalues. The LHC/FCC is insensitive towards the higher orders of precision, which allows us the freedom to fine-tune the entries.

BP1.—The choice of Yukawa couplings for BP1 are as follows:

$$\mathcal{Y}_1^L = \begin{pmatrix} 0.220 & 0.001 & -0.030 \\ 0.150 & -0.005 & 0.140 \\ 0.005 & 0.120 & 0.006 \end{pmatrix};$$
$$\mathcal{Y}_1^R = \begin{pmatrix} 1.000 & 0.000 & 0.000 \\ 0.150 & 0.000 & 0.200 \\ 0.000 & 0.120 & 0.009 \end{pmatrix};$$
$$\mathcal{Y}_2 = 10^{-3} \begin{pmatrix} 0.00000 & -0.03900 & -0.00082 \\ 0.28200 & 0.00000 & 0.00000 \\ 0.35900 & 0.01810 & 0.00000 \end{pmatrix}. \quad (3.1)$$

In this scenario, the tiny values of $\mathcal{Y}_2$ makes $\tilde{R}_2$ almost inert and therefore the total decay width of $\tilde{R}_2^{+2/3}$ becomes very small, i.e. 6.27×10^{-6} GeV, but large enough to create prompt decays. Due to this fact the dynamics of

TABLE II. Dominant decay modes and branching ratios of the three leptoquark eigenstates for BP1.

Dominant decay modes of leptoquarks for BP1								
$\tilde{R}_2^{+2/3}$ $m(\tilde{R}_2^{2/3}) = 1.502$ TeV			$X_1^{-1/3}$ $M_1 = 1.499$ TeV			$X_2^{-1/3}$ $M_2 = 1.506$ TeV		
$\Gamma(\tilde{R}_2^{2/3}) = 6.27 \times 10^{-6}$ GeV			$\Gamma(X_1) = 25.6$ GeV			$\Gamma(X_2) = 13.0$ GeV		
Mode	Dominant Yukawa	BR (%)	Mode	Dominant Yukawa	BR (%)	Mode	Dominant Yukawa	BR (%)
be^+	$(\mathcal{Y}_2)_{31}$	61.6	ue^-	$(\mathcal{Y}_1^R)_{11} + (\tilde{\mathcal{Y}}_1^L)_{11}$	82.4	ue^-	$(\mathcal{Y}_1^R)_{11} + (\tilde{\mathcal{Y}}_1^L)_{11}$	82.4
se^+	$(\mathcal{Y}_2)_{21}$	37.5	$c\tau^-$	$(\mathcal{Y}_1^R)_{23} + (\tilde{\mathcal{Y}}_1^L)_{23}$	4.6	$c\tau^-$	$(\mathcal{Y}_1^R)_{23} + (\tilde{\mathcal{Y}}_1^L)_{23}$	4.6
			$d\nu_e$	$(\mathcal{Y}_1^L)_{11}$	3.8	$d\nu_e$	$(\mathcal{Y}_1^L)_{11}$	3.8

TABLE III. Dominant decay modes and branching ratios of the three leptoquark eigenstates for BP2.

Dominant decay modes of leptoquarks for BP2								
$\tilde{R}_2^{+2/3}$ $m(\tilde{R}_2^{2/3}) = 1.502$ TeV			$X_1^{-1/3}$ $M_1 = 1.499$ TeV			$X_2^{-1/3}$ $M_2 = 1.506$ TeV		
$\Gamma(\tilde{R}_2^{2/3}) = 9.76 \times 10^{-1}$ GeV			$\Gamma(X_1) = 30.3$ GeV			$\Gamma(X_2) = 15.9$ GeV		
Mode	Dominant Yukawa	BR (%)	Mode	Dominant Yukawa	BR (%)	Mode	Dominant Yukawa	BR (%)
se^+	$(\mathcal{Y}_2)_{21}$	63.5	$u\mu^-$	$(\mathcal{Y}_1^R)_{12} + (\tilde{\mathcal{Y}}_1^L)_{12}$	32.7	$u\mu^-$	$(\mathcal{Y}_1^R)_{12} + (\tilde{\mathcal{Y}}_1^L)_{12}$	31.7
be^+	$(\mathcal{Y}_2)_{31}$	36.3	$c\mu^-$	$(\mathcal{Y}_1^R)_{22} + (\tilde{\mathcal{Y}}_1^L)_{22}$	32.7	$c\mu^-$	$(\mathcal{Y}_1^R)_{22} + (\tilde{\mathcal{Y}}_1^L)_{22}$	31.7
			$s\nu_\mu$	$(\mathcal{Y}_1^L)_{22}$	23.5	$s\nu_\mu$	$(\mathcal{Y}_1^L)_{22}$	22.8
			$d\nu_\mu$	$(\mathcal{Y}_1^L)_{12}$	9.2	$d\nu_\mu$	$(\mathcal{Y}_1^L)_{12}$	8.9

$X_1^{-1/3}$ and $X_2^{-1/3}$ are mostly dominated by the singlet component S_1. The mass eigenstates of the leptoquarks with charge 1/3, i.e. $X_{1,2}^{-1/3}$, are almost degenerate with a mass difference of ∼7 GeV; however, the total decay width of X_1 is approximately twice that of X_2. The branching fractions of the leptoquarks in their mass basis, for different modes are presented in Table II. Among all the components of $\mathcal{Y}_1^L$ and $\mathcal{Y}_1^R$, the large $(\mathcal{Y}_1^R)_{11} = 1.0$ makes ue the dominant decay channel of $X_{1,2}^{-1/3}$ with 82.4% of the branching fraction. The doublet Yukawa $\mathcal{Y}_2$ has a negligible effect on their branching, and only governs the decay modes of $\tilde{R}_2^{+2/3}$.

BP2.—For this benchmark point, the $\mathcal{Y}_1^L$ and $\mathcal{Y}_1^R$ Yukawa couplings are chosen in such a way that, for $X_1^{-1/3}$ and $X_2^{-1/3}$ leptoquarks, we can obtain more than one dominant decay mode with comparable branching fractions, unlike in BP1. The structures of these couplings are given below:

$$\mathcal{Y}_1^L = \begin{pmatrix} 0.0000 & 0.3740 & -0.0100 \\ -0.0008 & 0.5990 & 0.0420 \\ 0.0200 & 0.0223 & 0.0418 \end{pmatrix};$$
$$\mathcal{Y}_1^R = \begin{pmatrix} 0.00 & 0.50 & 0.00 \\ 0.00 & 0.50 & 0.05 \\ 0.02 & 0.00 & 0.03 \end{pmatrix};$$
$$\mathcal{Y}_2 = 10^{-3} \begin{pmatrix} 5.0000 & -1.1893 & -1.3230 \\ -144.0400 & 5.0000 & -2.1195 \\ -108.8400 & 5.0363 & 0.0000 \end{pmatrix}. \quad (3.2)$$

The total decay widths and branching fractions of all the leptoquarks under this BP are listed in Table III. In this case, the total decay width of $\tilde{R}_2^{+2/3}$ gets enhanced to ∼1 GeV, due to larger values of $(\mathcal{Y}_2)_{21}$ and $(\mathcal{Y}_2)_{31}$, i.e. $\mathcal{O}(10^{-1})$, compared to the BP1 scenario, where the total decay width is $\mathcal{O}(10^{-6})$ GeV. Owing to the larger values of $(\mathcal{Y}_2)_{21}$ and $(\mathcal{Y}_2)_{31}$, $\tilde{R}_2^{+2/3}$ decays dominantly to se^+ (63.5%) and be^+ (36.3%). The mass splitting and the ratio of the total decay widths between X_1 and X_2 remain similar as BP1. However, for this particular choice of $\mathcal{Y}_1^{R,L}$, $X_1^{-1/3}$ and $X_2^{-1/3}$ both dominantly decay to $u\mu$ and $c\mu$, with equal branching fractions of 32.7% in the case of $X_1^{-1/3}$, and 31.7% in the case of $X_2^{-1/3}$, respectively. This is attributed to the fact that, while we already have $(\mathcal{Y}_1^R)_{12} = (\mathcal{Y}_1^R)_{22} = 0.5$, after the CKM rotation of $\mathcal{Y}_1^L$ we also get $(\tilde{\mathcal{Y}}_1^L)_{12} = (\tilde{\mathcal{Y}}_1^L)_{22} \approx 0.5$. Additionally, two other significant decay modes of $X_{1,2}^{-1/3}$ open up, namely $s\nu$ (∼23%) and $d\nu$ (∼9%).

BP3.—For the third benchmark points, we wish to have significantly different branching ratios for $X_1^{-1/3}$ and $X_2^{-1/3}$, contrary to the two previous scenarios. Hence, the Yukawa couplings for this BP are chosen as follows:

$$\mathcal{Y}_1^L = \begin{pmatrix} -0.0070 & 0.0490 & 0.4870 \\ 0.0290 & 0.0092 & 0.1124 \\ 0.0012 & 0.0500 & 0.0017 \end{pmatrix};$$
$$\mathcal{Y}_1^R = \begin{pmatrix} 0.0 & 0.5 & 0.5 \\ 0.5 & 0.0 & 0.0 \\ 0.0 & 0.3 & 0.0 \end{pmatrix};$$
$$\mathcal{Y}_2 = 10^{-3} \begin{pmatrix} 0.00000 & 878.31000 & -2.62350 \\ -2.03300 & 200.00000 & -0.48457 \\ 89.30000 & 3.00000 & -2.67500 \end{pmatrix}. \quad (3.3)$$

The branching fractions for the leptoquark mass eigenstates are depicted in Table IV. As a result of the large $(\mathcal{Y}_2)_{12}$ and $(\mathcal{Y}_2)_{22}$, the total decay width of $\tilde{R}_2^{+2/3}$ in this scenario, i.e. 24.4 GeV, becomes comparable to that of $X_{1,2}^{-1/3}$. Because of the same fact, the branching fractions of $X_1^{-1/3}$ and $X_2^{-1/3}$ look quite different, since $X_1^{-1/3}$ and $X_2^{-1/3}$ contain different proportions of S_1 and $\tilde{R}_2^{1/3}$. Here, the total decay widths of $X_1^{-1/3}$ and $X_2^{-1/3}$ are also quite close unlike the previous two cases, as a result of both $\mathcal{Y}_1^R$ and $\mathcal{Y}_2$ containing entries of $\mathcal{O}(10^{-1})$. The element $(\mathcal{Y}_2)_{12} = 0.876269$ results in $\tilde{R}_2^{+2/3}$ decaying dominantly to $d\mu^+$

TABLE IV. Dominant decay modes and branching ratios of the three leptoquark eigenstates for BP3.

Dominant decay modes of leptoquarks for BP3								
$\tilde{R}_2^{+2/3}$ $m(\tilde{R}_2^{2/3}) = 1.502$ TeV			$X_1^{-1/3}$ $M_1 = 1.499$ TeV			$X_2^{-1/3}$ $M_2 = 1.506$ TeV		
$\Gamma(\tilde{R}_2^{+2/3}) = 24.4$ GeV			$\Gamma(X_1) = 34.9$ GeV			$\Gamma(X_2) = 29.8$ GeV		
Mode	Dominant Yukawa	BR (%)	Mode	Dominant Yukawa	BR (%)	Mode	Dominant Yukawa	BR (%)
$d\mu^+$	$(\mathcal{Y}_2)_{12}$	94.1	$u\tau^-$	$(\mathcal{Y}_1^R)_{13} + (\tilde{\mathcal{Y}}_1^L)_{13}$	28.4	$d\bar{\nu}_\mu$	$(\mathcal{Y}_2)_{12}$	51.4
$s\mu^+$	$(\mathcal{Y}_2)_{22}$	4.9	$d\bar{\nu}_\mu$	$(\mathcal{Y}_2)_{12}$	22.2	$u\tau^-$	$(\mathcal{Y}_1^R)_{13} + (\tilde{\mathcal{Y}}_1^L)_{13}$	16.9
			$u\mu^-$	$(\mathcal{Y}_1^R)_{12} + (\tilde{\mathcal{Y}}_1^L)_{12}$	14.3	$u\mu^-$	$(\mathcal{Y}_1^R)_{12} + (\tilde{\mathcal{Y}}_1^L)_{12}$	8.5
			ce^-	$(\mathcal{Y}_1^R)_{21} + (\tilde{\mathcal{Y}}_1^L)_{21}$	14.2	ce^-	$(\mathcal{Y}_1^R)_{21} + (\tilde{\mathcal{Y}}_1^L)_{21}$	8.4
			$d\bar{\nu}_\tau$	$(\mathcal{Y}_1^L)_{13}$	13.5	$d\bar{\nu}_\tau$	$(\mathcal{Y}_1^L)_{13}$	8.0

with a branching fraction of 94.1%. As the X_2 leptoquark contains 66% of $\tilde{R}_2^{-1/3}$, so this same large coupling enhances the decay of $X_2^{-1/3} \to d\nu_\mu$, with a 51.4% branching fraction. The other decay modes of $X_2^{-1/3}$ are dominated by $\mathcal{Y}_1^{L,R}$, the larger of them being $u\tau$ (16.9%). On the other hand, as $X_1^{-1/3}$ contains 66% of S_1, the largest branching fraction is observed in the $u\tau$ decay channel (28.4%). However, the larger value of $(\mathcal{Y}_2)_{12}$ still affects its decay, owing to the 33.5% of $\tilde{R}_2^{-1/3}$ remaining in it. This results in the 22.2% branching fraction of $X_1^{-1/3}$ decaying to $d\nu_\mu$. However, significant difference between the BRs of $X_{1,2}^{-1/3} \to d\nu_\mu$ is observed, which is the purpose of choosing the Yukawa couplings as described in Eq. (3.3).

B. Neutrino mass from the chosen BPs

Following the discussion on our choice of Yukawa couplings and their effect on the leptoquark decay channels, we will now look into the experimental bounds on various low-energy observables and their corresponding values under these benchmark scenarios. The first motivation of choosing this model containing a doublet and a singlet leptoquark was to generate neutrino masses at one loop. It turns out that, up to the stated accuracy of the Yukawa coupling entries, the neutrino mass eigenvalues shape up as depicted in Table V. though there is no bound on individual masses of active neutrinos, their total mass should be less than 0.09 eV [18]. We observe that, in all three benchmark points, the neutrino mass sum stays within a value of 0.075 eV.

The next immediate bounds comes from the neutrino mass-squared differences. It is important to note that, for the purpose of this work, the normal hierarchy of neutrino mass is considered, where $m_{\nu_3} > m_{\nu_2} > m_{\nu_1}$ [176]. However, one can choose to work with the inverted hierarchy as well, tweaking the parameter space as required. In consideration of the normal hierarchy, the respective mass-squared differences and the experimental 3σ range are provided in Table VI. Up to the quoted order of precision, the entries of the Yukawa coupling matrices results into values within the allowed 3σ range.

However, further fine-tuning at least at the third decimal point of the chosen Yukawa couplings is unavoidable to fully satisfy the neutrino oscillation parameters within the 3σ range, which we will discuss towards the end of this section.

C. Muon and electron $g-2$ from the chosen BPs

With the help of SPheno, it is observed that the benchmark points up to the stated accuracy also satisfy the muon and electron $g-2$ data [41,53,54]. The experimental results for these observables and their values under our choice of benchmark points are listed in Table VII. It should be noticed that the values of the electron $g-2$ for our BPs are more in accordance with the experimental values for rubidium, which is the more recent measurement.

TABLE V. Masses of neutrinos under different benchmark points and experimental bound.

Parameter	Experimental bound	BP1	BP2	BP3
m_{ν_1} (eV)	⋯	0.009	0.010	0.009
m_{ν_2} (eV)	⋯	0.012	0.013	0.013
m_{ν_3} (eV)	⋯	0.051	0.052	0.052
$\sum m_\nu$ (eV)	< 0.09 [18]	0.072	0.075	0.074

TABLE VI. Neutrino mass-squared differences for the three benchmark points, along with the experimental 3σ values (normal hierarchy).

Parameter	Experimental 3σ range	BP1	BP2	BP3
$\Delta m_{21}^2 (\times 10^{-5}\ \text{eV}^2)$	6.94–8.14	7.03	7.84	8.12
$\Delta m_{31}^2 (\times 10^{-3}\ \text{eV}^2)$	2.47–2.63	2.47	2.63	2.63

TABLE VII. Experimental estimates of muon and electron $(g-2)$ and their values for the three benchmark points, given by SPHENO.

Observable	Experimental value	BP1	BP2	BP3
Δa_μ	$(2.51 \pm 0.59) \times 10^{-9}$ [41]	2.97×10^{-9}	2.44×10^{-9}	3.10×10^{-9}
Δa_e^{Cs}	$(-8.8 \pm 3.6) \times 10^{-13}$ [53]	7.71×10^{-13}	4.00×10^{-13}	7.02×10^{-13}
Δa_e^{Rb}	$(4.8 \pm 3.0) \times 10^{-13}$ [54]			

D. Fine-tuning of the BPs

Having discussed the bounds that are satisfied with the lowest possible precision of the Yukawa couplings, we now move towards the fine-tuning of the same, through which the neutrino oscillation data and the CLFV observables can also be addressed. The fine-tunings are required mainly for $\mathcal{Y}_1^L$ and $\mathcal{Y}_2$, at least at the third decimal place, as these two Yukawa couplings contribute towards the neutrino mass and mixing. For our purpose, $\mathcal{Y}_1^R$ does not require any such fine-tuning. It is important to note that, from the perspective of analysis at the LHC/FCC, such fine-tuned precise values of the couplings do not affect the observations of the final states. As we have seen from the discussion on the decay branching ratios in Sec. III A, only the entries of $\mathcal{O}(10^0$–$10^{-1})$ lead to significantly observable decay channels. Therefore, fine-tuning at $\mathcal{O}(10^{-3})$ or less does not affect the collider study. Nonetheless, such minute adjustments at $\mathcal{O}(\lesssim 10^{-3})$ are inevitable for us to be consistent with the neutrino oscillation and CLFV bounds. Below, we list the high-precision values of the Yukawa couplings in the three aforementioned benchmark points.

BP1.—

$$\mathcal{Y}_1^L = \begin{pmatrix} 0.221039 & 0.000714 & -0.031542 \\ 0.153678 & -0.004908 & 0.136279 \\ 0.004975 & 0.119897 & 0.005766 \end{pmatrix}; \qquad \mathcal{Y}_1^R = \begin{pmatrix} 1.000 & 0.000 & 0.000 \\ 0.150 & 0.000 & 0.200 \\ 0.000 & 0.120 & 0.009 \end{pmatrix};$$
$$\mathcal{Y}_2 = 10^{-3} \begin{pmatrix} 0.000000000 & -0.038621100 & -0.000825144 \\ 0.280505000 & 0.000000000 & 0.0000224450 \\ 0.359512000 & 0.018091600 & 0.000000000 \end{pmatrix}. \tag{3.4}$$

BP2.—

$$\mathcal{Y}_1^L = \begin{pmatrix} 0.000119 & 0.374489 & -0.009901 \\ -0.000818 & 0.599381 & 0.042168 \\ 0.019983 & 0.022305 & 0.041819 \end{pmatrix}; \qquad \mathcal{Y}_1^R = \begin{pmatrix} 0.00 & 0.50 & 0.00 \\ 0.00 & 0.50 & 0.05 \\ 0.02 & 0.00 & 0.03 \end{pmatrix};$$
$$\mathcal{Y}_2 = 10^{-3} \begin{pmatrix} 5.00000 & -1.17252 & -1.31907 \\ -144.02600 & 5.00000 & -2.11232 \\ -108.86400 & 5.01788 & 0.00000 \end{pmatrix}. \tag{3.5}$$

BP3.—

$$\mathcal{Y}_1^L = \begin{pmatrix} -0.00675900 & 0.04901100 & 0.48713800 \\ 0.02920300 & 0.00922200 & 0.11267200 \\ 0.00123556 & 0.05012900 & 0.00171300 \end{pmatrix}; \qquad \mathcal{Y}_1^R = \begin{pmatrix} 0.0 & 0.5 & 0.5 \\ 0.5 & 0.0 & 0.0 \\ 0.0 & 0.3 & 0.0 \end{pmatrix};$$
$$\mathcal{Y}_2 = 10^{-3} \begin{pmatrix} 0.0000000 & 876.2690000 & -2.6172423 \\ -1.9016000 & 200.0000000 & -0.4845686 \\ 87.8210000 & 3.0095000 & -2.6750000 \end{pmatrix}. \tag{3.6}$$

TABLE VIII. Neutrino oscillation data (normal ordering) [176] and values of oscillation parameters under different benchmark points.

Parameter	Experimental 3σ range	BP1	BP2	BP3
$\sin^2\theta_{12}$	0.27–0.37	0.27	0.30	0.31
$\sin^2\theta_{13}$	0.020–0.024	0.023	0.023	0.023
$\sin^2\theta_{23}$	0.43–0.61	0.50	0.59	0.59
δ_{CP}	120°–369°	180°	180°	180°
U_{11}	$0.801 < \lvert U_{11}\rvert < 0.845$	−0.844	0.830	−0.823
U_{12}	$0.513 < \lvert U_{12}\rvert < 0.579$	−0.514	0.537	−0.547
U_{13}	$0.143 < \lvert U_{13}\rvert < 0.155$	0.152	0.150	0.153
U_{21}	$0.234 < \lvert U_{21}\rvert < 0.500$	0.276	−0.252	0.256
U_{22}	$0.471 < \lvert U_{22}\rvert < 0.689$	−0.661	0.601	−0.598
U_{23}	$0.637 < \lvert U_{23}\rvert < 0.776$	−0.698	−0.758	−0.759
U_{31}	$0.271 < \lvert U_{31}\rvert < 0.525$	−0.459	0.498	−0.507
U_{32}	$0.477 < \lvert U_{32}\rvert < 0.694$	0.547	−0.591	0.586
U_{33}	$0.613 < \lvert U_{33}\rvert < 0.756$	−0.700	0.634	−0.632

With the values of the Yukawa couplings modified to higher orders of precision, we obtain the neutrino oscillation parameters as depicted in Table VIII for the three fine-tuned BPs, along with the experimental 3σ ranges. As we are working with real Yukawa couplings, the CP-violating phase δ_{CP} is chosen to be 180°, for convenience, so that the PMNS mixing matrix also becomes real. The 3σ range of the absolute value for each component of the 3×3 PMNS matrix, denoted as U_{ij}, are also presented in Table VIII.

Finally, we consider the constraints from various CLFV processes, for which the experimental bounds, along with their values under three benchmark points of this model, are presented in Table IX. The tightest constraint comes from the $\mu \to e\gamma$ by the MEG collaboration [177] providing the branching fraction to be smaller than 4.2×10^{-13}. Experiment Sindrum II dealing with μ-e conversion by gold atom puts another stringent bound stating that the branching ratio of this process with respect to the nuclear capture probability should be less than 7×10^{-13} [178]. The other bounds are not very strong relative to these two and are automatically satisfied. For our simulation we generated all these results through SPheno.

IV. COLLIDER PHENOMENOLOGY

After setting up the model and the benchmark scenarios in the previous sections, we now perform a series of simulations to probe this model at the current 14 TeV LHC, as well as the future HL/HE-LHC and the FCC. In this section, we will be studying the pair production of the

TABLE IX. Bounds on various LFV processes and their SPheno generated values for different benchmark points.

No.	CLFV mode	Experimental branching	BP1	BP2	BP3
1	$\mu \to e\gamma$	$<4.2\times 10^{-13}$	9.19×10^{-14}	3.36×10^{-15}	5.09×10^{-15}
2	$\tau \to e\gamma$	$<3.3\times 10^{-8}$	3.04×10^{-8}	3.18×10^{-8}	6.36×10^{-17}
3	$\tau \to \mu\gamma$	$<4.4\times 10^{-8}$	3.71×10^{-8}	4.10×10^{-8}	4.53×10^{-10}
4	$\mu \to 3e$	$<1.0\times 10^{-12}$	6.46×10^{-16}	8.57×10^{-15}	3.93×10^{-16}
5	$\tau \to 3e$	$<2.7\times 10^{-8}$	4.08×10^{-10}	3.83×10^{-10}	2.47×10^{-17}
6	$\tau \to 3\mu$	$<2.1\times 10^{-8}$	9.56×10^{-11}	1.49×10^{-10}	8.55×10^{-10}
7	$\mu - e$, Ti	$<4.3\times 10^{-12}$	2.19×10^{-13}	6.34×10^{-13}	5.66×10^{-13}
8	$\mu - e$, Au	$<7\times 10^{-13}$	2.38×10^{-13}	6.31×10^{-13}	6.29×10^{-13}
9	$\mu - e$, Pb	$<4.6\times 10^{-11}$	2.30×10^{-13}	6.04×10^{-13}	6.08×10^{-13}
10	$\tau^- \to e^-\mu^+\mu^-$	$<2.7\times 10^{-8}$	8.78×10^{-11}	7.53×10^{-11}	7.02×10^{-17}
11	$\tau^- \to \mu^- e^+ e^-$	$<1.8\times 10^{-8}$	4.39×10^{-10}	5.04×10^{-10}	5.30×10^{-10}
12	$\tau^- \to e^+\mu^-\mu^-$	$<1.7\times 10^{-8}$	2.71×10^{-30}	1.84×10^{-25}	1.12×10^{-22}
13	$\tau^- \to \mu^+ e^- e^-$	$<1.5\times 10^{-8}$	2.92×10^{-27}	2.08×10^{-22}	1.07×10^{-24}
14	$Z \to e\mu$	$<7.5\times 10^{-7}$	7.81×10^{-23}	4.91×10^{-17}	5.23×10^{-19}
15	$Z \to e\tau$	$<9.8\times 10^{-6}$	3.12×10^{-13}	4.87×10^{-14}	1.56×10^{-18}
16	$Z \to \mu\tau$	$<1.2\times 10^{-5}$	5.87×10^{-14}	5.36×10^{-13}	1.05×10^{-11}
17	$h \to e\mu$	$<6.1\times 10^{-5}$	3.16×10^{-18}	1.13×10^{-19}	1.12×10^{-20}
18	$h \to e\tau$	$<4.7\times 10^{-3}$	3.11×10^{-12}	1.75×10^{-9}	6.70×10^{-21}
19	$h \to \mu\tau$	$<2.5\times 10^{-3}$	2.02×10^{-9}	4.14×10^{-12}	6.01×10^{-16}

three leptoquark (LQ) eigenstates of $\tilde{R}_2^{+2/3}$ and $X_{1,2}^{-1/3}$ from proton-proton collisions at three different center-of-mass energies (E_{CM}) of 14, 27 and 100 TeV, respectively.

A. Simulation at the LHC/FCC: Setup

For the simulations at the LHC/FCC, the hard scattering event files are generated in the `.lhe` format from CalcHEP [179] version 3.8.7.SPheno version 4.0.4 is utilized to obtain spectrum files (`.spc` format) to be read by CalcHEP as parameter cards. The parton shower, hadronization and jet clustering are done with PYTHIA 8.2.45 [180]. To form the jets, FASTJET-3.3.3 [181] is used with the Cambridge-Aachen jet clustering algorithm [182] with a jet radius of 0.5. the same softwares and parameters are utilized to simulate the five dominant SM backgrounds (BGs) at the LHC, namely $t\bar{t}$, VV, VVV, $t\bar{t}V$, and tVV (where V represents the electroweak vector bosons W/Z), so that we can compare the signal events with the background to obtain the significance of discovery. The next-to-leading order (NLO) K factors for the backgrounds are calculated with MadGraph5_aMC@NLO version 3.1.0 [171]. Additionally, the following cuts are imposed:

(i) Calorimeter coverage, $|\eta| < 4.5$.
(ii) Transverse momentum cut for jets and leptons, $p_{T,\min}^{\text{jet,lep}} = 20.0$ GeV.
(iii) Leptons are hadronically cleaned, with minimized hadronic activity within a cone of radius $\Delta R_{hl} = 0.3$ with the relation $\sum p_T^{\text{had}} = 0.15 p_T^{\text{lep}}$.
(iv) Leptons are isolated from jets, with a cone radius cut of $\Delta R_{lj} > 0.4$.
(v) Pertaining to the high mass of the leptoquarks, i.e. 1.5 TeV in the benchmark points, a cut on the total hardness of the event, defined as $p_T^H = \sum(p_T^{\text{lep}} + p_T^{\text{jet}} + \not{p}_T) \geq 1.2$ TeV, is applied to both the signal and background events, at the analysis level. Additionally, for convergence of the events at the high-momentum tail, the SM background events are generated with a phase space cut of $\sqrt{\hat{s}} \geq 1.2$ TeV.
(vi) For further filtering of the backgrounds, the following dijet and dilepton invariant mass vetoes are imposed: $|M_{jj} - M_Z| \geq 10$ GeV, $|M_{jj} - M_W| \geq 10$ GeV, and $|M_{\ell\ell} - M_Z| \geq 10$ GeV.

Moreover, for ease of analysis and clarity of signal, we perform flavor tagging of heavy jets. For b tagging, we take the efficiency to be ∼70% following a secondary vertex reconstruction algorithm [183]. For c tagging we consider a conservative efficiency of ∼56% with a misidentification rate of ∼0.12 [184]. Again, while tagging the τ jets using one- or three-prong $\pi^{\pm}$ tracks, we take the hadronic τ-jet identification efficiency of ∼75% for a misidentification rate of $\sim 10^{-2}$, as reported in [185]. With this setup, we are now ready to move ahead with our simulations of leptoquark pair production.

B. Leptoquark pair production

For the pair production of LQs in pp collisions, we are considering the QCD processes, along with the contribution from t-channel lepton exchange diagrams as shown in Fig. 3. The QCD dominated leading-order partonic cross section for the pair production of scalar leptoquarks through gluon and quark fusion channels can be expressed as [125,156]

$$\hat{\sigma}_{gg} = \frac{\pi\alpha_s^2}{96\hat{s}}\left[\beta(41 - 31\beta^2) - (17 - 18\beta^2 + \beta^4)\log\left|\frac{1+\beta}{1-\beta}\right|\right]$$
$$\text{and} \quad \hat{\sigma}_{q\bar{q}} = \frac{2\pi\alpha_s^2}{27\hat{s}}\beta^3, \tag{4.1}$$

where $\beta = \sqrt{1 - 4M_{LQ}^2/\hat{s}}$ with M_{LQ} being the mass of the leptoquark, $\hat{s}$ the partonic center-of-mass energy and α_s the strong coupling constant. As shown in Ref. [156], the effect of the t-channel lepton exchange diagram becomes

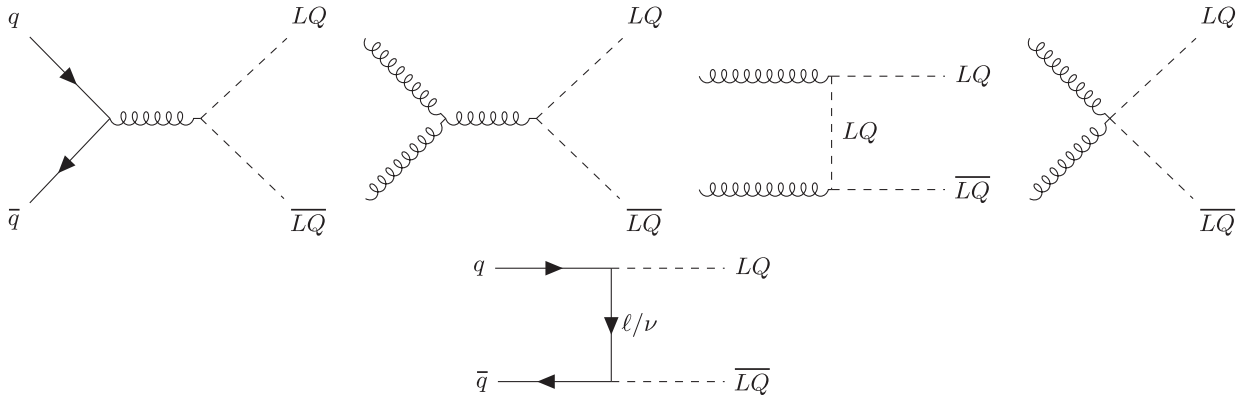

FIG. 3. Feynman diagrams for pair production of leptoquarks from pp collisions at the LHC.

TABLE X. Production cross sections of leptoquark pairs from pp collisions at the LHC at $E_{CM} = 14$, 27 and 100 TeV, with `cteq6l1` as PDF, and the NLO K factor $= 2.02$.

	$pp \to LQ\overline{LQ}$ at different E_{CM}s								
	$\sigma_{\tilde{R}_2^{2/3}\tilde{R}_2^{-2/3}}$ (fb)			$\sigma_{X_1^{1/3}X_1^{-1/3}}$ (fb)			$\sigma_{X_2^{1/3}X_2^{-1/3}}$ (fb)		
BPs	14 TeV	27 TeV	100 TeV	14 TeV	27 TeV	100 TeV	14 TeV	27 TeV	100 TeV
BP1	0.39	10.91	779.3	0.61	15.21	890.8	0.35	10.53	772.8
BP2	0.39	10.91	779.6	0.32	10.13	778.5	0.32	9.90	755.5
BP3	0.54	14.70	886.5	0.30	9.80	770.0	0.33	10.48	780.9

significant only when the scattering angle is very small. However, to obtain the total cross section for the pair production of leptoquarks at the hadronic collider, one has to wrap each of the partonic cross sections with a parton distribution function (PDF) and sum over all the different contributions.

The leptoquark model is implemented in SARAH [168], and model files for CalcHEP [179] are generated from there. Reading the parameter cards from SPheno, CalcHEP evaluates the pair production cross sections at leading order (LO) QCD, taking the `cteq6l1` parton distribution function (PDF) [186]. However, we wish to perform our pair production analysis at the next-to-leading order (NLO) QCD. For that, we first neglect the lepton exchange diagrams to match the cross sections with the published results from [130,187] and make a judicial choice of NLO QCD K-factor $= 1.84$ for $M_{LQ} = 1.5$ TeV. Next we include the t-channel lepton exchange diagrams along with the QCD processes, where the BPs with $\mathcal{O}(1)$ Yukawa couplings can have some significant effect on the total cross section. Referring to the results published in [91,188], it is observed that, for 1.5 TeV leptoquark mass, the ratio of cross sections at NLO QCD with both QCD-mediated + t-channel lepton processes, compared to only QCD processes without t channel, come out to be about 1.1. Therefore, our effective K factor now becomes $1.84 \times 1.1 \approx 2.02$. Moreover, the cross sections are evaluated at the renormalization scale $\mu_R = M_{LQ} = 1.5$ TeV, at which the value of strong coupling α_S for `cteq6l1` PDF is 0.0899.

With this setup of parameters, we evaluate the cross sections at three different center-of-mass energies (E_{CM}) of 14, 27 and 100 TeV, corresponding to present and future iterations of the LHC/FCC. These cross sections for the three benchmark points are presented in Table X. From this table we note that, in the case of BP1, the X_1 pair production cross section is large due to $(\mathcal{Y}_1^R)_{11} = 1.0$, while in BP3, $\tilde{R}_2$ pair production is enhanced by the dominance of $(\mathcal{Y}_2)_{12} = 0.876$. In BP2, the slight difference in cross sections of $X_{1,2}$ pair production is resulting from the small mass gap of $M_{X_1} - M_{X_2} \approx 7$ GeV. The effect of this mass gap is overcome by the $(\mathcal{Y}_2)_{12} = 0.876$ in BP3, which enhances the cross section for $X_2^{-1/3}$ slightly higher than $X_1^{-1/3}$, despite being heavier.

In Table XI, we illustrate the effective branching fractions of different observable final states at the LHC/FCC, in accordance with the Yukawa couplings and decay channels discussed in Sec. III. Here, $\not{p}_T$ refers to the missing transverse momentum that is carried by particles such as neutrinos which are not observable at the LHC, and OS means "oppositely signed." The light jets, i.e. non-flavor-tagged jets, are represented as j. The final states and probabilities for $\tilde{R}_2^{+2/3}$ pair production look very different than those of $X_{1,2}^{-1/3}$, due to the difference in charge, as well as for $\tilde{R}_2^{+2/3}$ being purely doublet. In BP1 and BP2, the mixed states $X_{1,2}^{-1/3}$ have almost the same probabilities for their final states, which are governed mostly by $\mathcal{Y}_1^{L,R}$. In the case of BP3, the effect of $\mathcal{Y}_2$ comes into play, leading to different probabilities for the same final states. We will be extensively using Table XI in the collider analysis that follows, in order to decide upon which final states to look for. The first objective for us is to probe the model at the LHC/FCC, and obtain a model signature with $\geq 5\sigma$ significance from the pair production events of all three leptoquark mass eigenstates. This study is discussed in detail in the following subsections.

C. Model signatures

To explore the feasibility of probing the model at the LHC/FCC, we first identify final states that are observable across all the three benchmark points. These final states also need to be direct consequences of the chosen Yukawa couplings, rather than emerging only due to initial- or final-state radiation (ISR, FSR) effects. To observe a significant excess of events over the SM backgrounds, we study the differential distributions of the kinematic variables pertaining to the emergent leptons and jets, so that some advanced cuts can be applied in our analysis.

1. Kinematics and final state topologies

In Fig. 4 the multiplicity distribution of isolated charged leptons emerging from the leptoquark pair production processes is presented, with panels (a)–(c) corresponding to BP1–BP3 respectively. The event numbers have been calculated with an integrated luminosity of 1000 fb^{-1}. Although the distributions are plotted for

TABLE XI. List of possible final states for pair production of leptoquarks at the LHC. Here, light jets are represented by j, OS refers to "opposite signed."

	Observable final states for different leptoquark pairs with effective branching ratios					
	$\tilde{R}_2^{2/3}\tilde{R}_2^{-2/3}$		$X_1^{1/3}X_1^{-1/3}$		$X_2^{1/3}X_2^{-1/3}$	
BPs	Final state	BR_{eff}	Final state	BR_{eff}	Final state	BR_{eff}
BP1	$2b$-jets $+ 2OSe$	0.38	$2j + 2OSe$	0.68	$2j + 2OSe$	0.68
	$1b$-jet $+ 1j + 2OSe$	0.46				
	$2j + 2OSe$	0.14				
BP2	$2j + 2OS\mu$	0.40	$2j + 2OS\mu$	0.11	$2j + 2OS\mu$	0.10
	$1b$-jet $+ 1j + 2OSe$	0.46	$1c$-jet $+ 1j + 2OS\mu$	0.21	$1c$-jet $+ 1j + 2OS\mu$	0.20
	$2b$-jets $+ 2OSe$	0.13	$2c$-jets $+ 2OS\mu$	0.11	$2c$-jets $+ 2OS\mu$	0.10
			$2j + \not{p}_T$	0.11	$2j + \not{p}_T$	0.10
			$1c$-jet $+ 1j + 1\mu + \not{p}_T$	0.21	$1c$-jet $+ 1j + 1\mu + \not{p}_T$	0.20
			$2j + 1\mu + \not{p}_T$	0.21	$2j + 1\mu + \not{p}_T$	0.20
BP3	$2j + 2OS\mu$	1.0	$2j + 2\tau$-jets	0.08	$2j + 2\tau$-jets	0.03
			$2j + 1\tau$-jet $+ \not{p}_T$	0.20	$2j + 1\tau$-jet $+ \not{p}_T$	0.20
			$2j + \not{p}_T$	0.13	$2j + \not{p}_T$	0.35
			$2j + 1\tau$-jet $+ 1\mu/e$	0.16	$2j + 1\tau$-jet $+ 1\mu/e$	0.06
			$2j + 2OS\mu e$	0.04	$2j + 2OS\mu e$	0.014
			$2j + 2OS\mu$	0.02	$2j + 2OS\mu$	0.007
			$2c$-jets $+ 2OSe$	0.02	$2c$-jets $+ 2OSe$	0.007
			$1j + 1c$-jet $+ 1\tau$-jet $+ 1e$	0.08	$1j + 1c$-jet $+ 1\tau$-jet $+ 1e$	0.03
			$2j + 1e/\mu + \not{p}_T$	0.20	$2j + 1e/\mu + \not{p}_T$	0.20

27 TeV center-of-mass energy owing to a larger number of events than for 14 TeV, the pattern of distributions do not alter much at 14 or 100 TeV energies. In each case, the green, yellow and pink bars correspond to $X_1^{-1/3}$, $X_2^{-1/3}$, and $\tilde{R}_2^{+2/3}$ pair productions, respectively. For each BP, the distributions for $\tilde{R}_2^{+2/3}$ preserve the same shape and they peak at $n_{\text{lep}} = 2$, which is obvious from the decay of the pair produced leptoquarks and also predicted by the effective branching fractions noted in Table XI. Depending on the dominant branching fractions of $X_{1,2}^{-1/3}$, the lepton multiplicity distribution varies for the three BPs. However, in all three cases this multiplicity becomes negligible for $n_{\text{lep}} > 2$, as there is no other possible source of leptons apart from the leptoquarks in the hard process. In BP1, the majority of events carry two leptons for both $X_{1,2}^{-1/3}$, due to a 68% probability of obtaining a $2j + \text{OS}e$ final state. In BP2 the multiplicity peaks at one lepton for both of these leptoquarks, with the numbers remaining almost the same for each. However, in BP3, even though pair production of both $X_1^{-1/3}$ and $X_2^{-1/3}$ leads to a majority of zero-lepton events, the ratios are not uniform unlike the other two BPs. The zero-lepton events are accounted for by the large branching ratios of $X_{1,2}^{-1/3}$ into neutrinos and τ jets. Such events are more dominant for $X_2^{-1/3}$, as a result of the greater probabilities of decaying into neutrinos and τ jets compared to $X_1^{-1/3}$, shown in Table XI.

Figure 5 depicts a similar comparative distribution of jet multiplicities for pair productions of $X_1^{-1/3}$ (green), $X_2^{-1/3}$ (yellow), and $\tilde{R}_2^{+2/3}$ (pink) leptoquarks, at $E_{CM} = 27$ TeV.

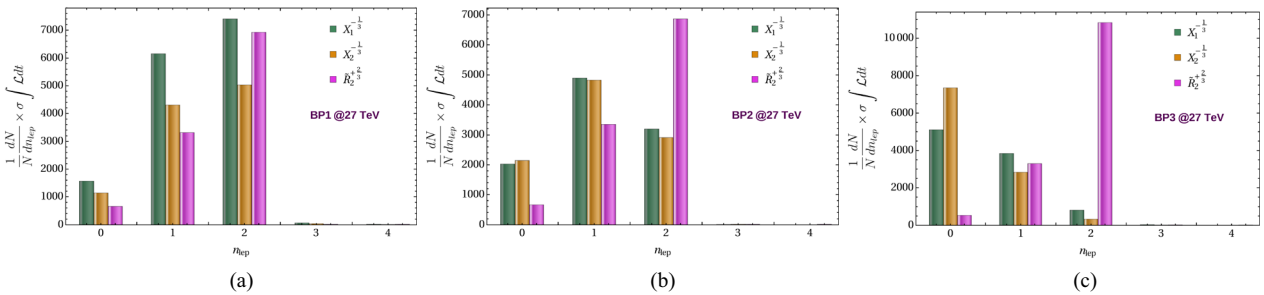

(a) (b) (c)

FIG. 4. Distribution of lepton multiplicity coming from pair production of $\tilde{R}_2^{+2/3}$ (pink) and $X_{1,2}^{-1/3}$ (green, yellow) for (a) BP1, (b) BP2, and (c) BP3, at the 27 TeV LHC.

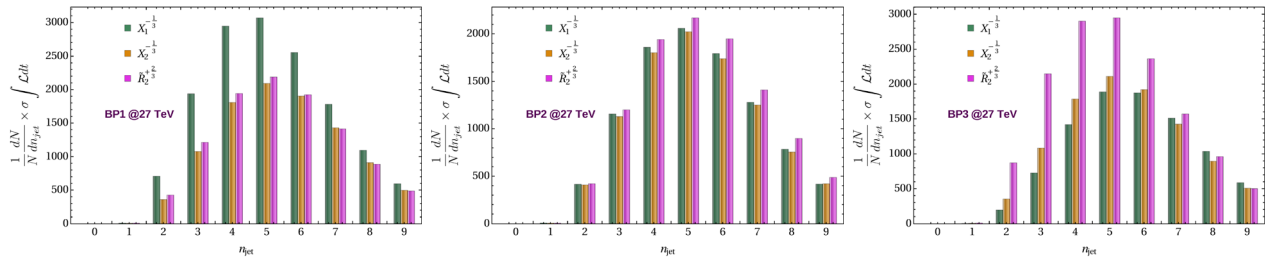

FIG. 5. Distribution of jet multiplicity coming from pair production of $\tilde{R}_2^{+2/3}$ (pink) and $X_{1,2}^{-1/3}$ (green, yellow) for (a) BP1, (b) BP2, and (c) BP3, at the 27 TeV LHC.

Here, irrespective of the benchmark point, we see very similar trends for all three leptoquarks. Although two hadronic jets are always expected from decays of a leptoquark and antileptoquark pair, the multiplicities actually peak at $n_{\rm jet} = 5$, owing to the ISR and FSR jets.

In Fig. 6, we portray the transverse momentum distributions of the hardest lepton emanating from each of the pair-produced leptoquarks $X_1^{-1/3}$ (green), $X_2^{-1/3}$ (yellow), and $\tilde{R}_2^{+2/3}$ (pink), at $E_{CM} = 27$ TeV for BP1 as well as from the SM background of $t\bar{t}$ (blue). Due to their nearly degenerate masses of ≈1.5 TeV, the p_T distributions for the leptons follow the same pattern for each leptoquark. Wide peaks are observed at around half the mass of the leptoquarks, signifying that the hardest leptons and jets are indeed arising from the decay of $\tilde{R}_2^{+2/3}$, $X_1^{-1/3}$ or $X_2^{-1/3}$. In the case of $t\bar{t}$, the lepton p_T peaks at roughly half of the $W^{\pm}$ boson mass, because the primary source of leptons in this case is the $W^{\pm}$ bosons resulting from the $t \to bW^{\pm}$ decays.

Now we look for the suitable final state topologies that can act as signatures for this doublet-singlet leptoquark extension of the SM. From Table XI we notice that, in each benchmark scenario, a final state of two light jets along with a pair of oppositely signed dileptons (OSD) is common between all three leptoquark mass eigenstates.

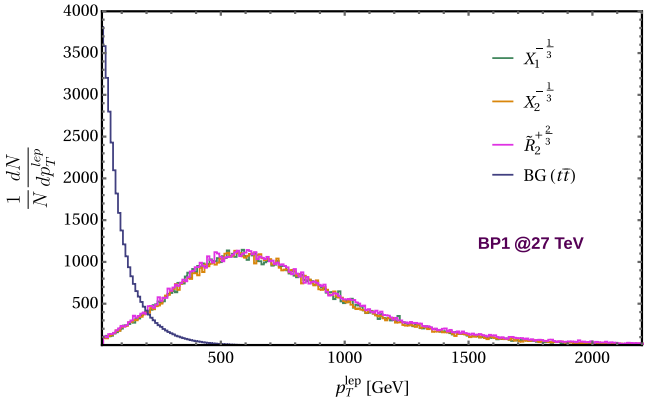

FIG. 6. The p_T distribution of the hardest lepton from the leptoquark pair productions, compared with that from the $t\bar{t}$ SM background.

However, for $\tilde{R}_2^{+2/3}$ in BP1 and BP2, a final state with two b-tagged jets and OSD is also highly probable. A similar observation is made for $X_1^{-1/3}$ and $X_2^{-1/3}$ with a topology of two c jets along with OSD. Therefore, after carefully observing the expected final states and probabilities from Table XI, we choose the two following topologies for our model signature:

$$\textbf{FS1}: n_{\rm jet} \geq 2 \quad \text{and} \quad n_{\ell^+} = n_{\ell^-} = 1 \quad \text{and} \quad n_{b/\tau\text{-jets}} = 0 \quad \text{and} \quad p_T^{\ell^+,\ell^-} \geq 300.0 \text{ GeV}, \tag{4.2}$$

and

$$\textbf{FS2}: n_{\rm jet} \geq 2 \quad \text{and} \quad n_{\ell^+} = n_{\ell^-} = 1 \quad \text{and} \quad n_{c/\tau\text{-jets}} = 0 \quad \text{and} \quad p_T^{\ell^+,\ell^-} \geq 300.0 \text{ GeV}. \tag{4.3}$$

Here, to obtain a cleaner signal by eliminating some background events, a 300 GeV cut on both the oppositely signed leptons' p_T has been implemented which is motivated by Fig. 6. The reason we demand the number of jets ≥ 2 rather than exactly equal to 2 is the fact that, as ISR and FSR increase the jet multiplicity, we do not wish to lose events by just looking at exactly two jets in the final state. In the next subsections, we will discuss the event numbers of these final states in detail.

2. 2 jets + 0 b/τ-jets + OSD

In Table XII we present the number of events obtained in the final state FS1 given by Eq. (4.2), for our three leptoquark pair production processes and the dominant SM backgrounds, at three different center-of-mass energies of 14, 27 and 100 TeV, at the LHC/FCC. In each of three benchmark points, all three leptoquark mass eigenstates lead to two light jets and two oppositely signed leptons, albeit with different probabilities. Additionally, in BP2 and BP3, the $X_{1,2}^{-1/3}$ leptoquarks decay to c jets, with probabilities of ∼10% in BP2 and ∼2% in BP2, for 2 c jets + OSD. We also veto out the events with any b- or τ-tagged jets for this final state. These observations are reflected in the observed number of events for the three benchmark scenarios. Contributing to availability of OSD

TABLE XII. The number of signal and background events for the topology FS1 in Eq. (4.2) for the pair production of the three leptoquarks at the LHC/FCC, across the three benchmark points. The numbers are presented for center-of-mass energies of 14, 27, and 100 TeV, with integrated luminosities of 3000, 1000 and 100 fb^{-1} for each E_{CM}, respectively. The signal significances and the required luminosities for a 5σ signal strength $\mathcal{L}_{5\sigma}$ are also presented.

		≥ 2 jets $+ 0\, b/\tau$-jets + OSD + $p_T^{\ell^+,\ell^-} \geq 300.0$ GeV							
		Signal			Backgrounds				
E_{CM} (TeV)	Pair produced leptoquark	BP1	BP2	BP3	$t\bar{t}$	VV	VVV	$t\bar{t}V$	tVV
14	$\tilde{R}_2^{+2/3}$	155.98	226.12	606.62					
	$X_1^{-1/3}$	445.53	143.65	28.30	246.63	202.17	17.80	2.53	0.0
	$X_2^{-1/3}$	241.62	136.48	11.10					
Total		843.13	506.25	646.02			469.13		
Significance		23.27σ	16.21σ	19.34σ					
$\mathcal{L}_{5\sigma}$(fb^{-1})		138.45	285.43	200.40					
27	$\tilde{R}_2^{+2/3}$	1235.47	1807.68	4944.14					
	$X_1^{-1/3}$	3279.64	1330.15	264.12	526.31	458.52	50.42	3.44	2.70
	$X_2^{-1/3}$	2085.87	1200.95	100.66					
Total		6600.98	4338.78	5308.92			1041.39		
Significance		75.51σ	59.15σ	66.62σ					
$\mathcal{L}_{5\sigma}$(fb^{-1})		4.97	7.14	5.63					
100	$\tilde{R}_2^{+2/3}$	7405.74	10931.30	24369.30					
	$X_1^{-1/3}$	15897.10	8695.07	1832.78	1172.99	731.67	111.14	8.39	4.43
	$X_2^{-1/3}$	12929.40	7802.14	680.35					
Total		36232.24	27428.51	26882.43			2028.62		
Significance		185.23σ	159.81σ	158.10σ					
$\mathcal{L}_{5\sigma}$(fb^{-1})		0.07	0.10	0.10					

and light jets, $t\bar{t}$ and diboson act as dominant SM background. As for the signal, BP1 receives the most contribution from $X_{1,2}^{-1/3}$, BP2 has $\tilde{R}_2^{+2/3}, X_{1,2}^{-1/3}$ contributing equivalently, and BP3 sees the majority of events from $\tilde{R}_2^{+2/3}$. At 14 TeV, the highest number of events in BP1 is observed for $X_1^{-1/3}$, owing to a larger cross section (Table X) and a ∼68% probability of leading to two light jets and OSD, as seen in Table XI. On the other hand, $X_2^{-1/3}$, having the same probability but less cross section, gives us the second largest number of events. Due to the absence of c jets as well as a less probability (∼14%) of $2j$ + OSD, the $\tilde{R}_2^{+2/3}$ pair production events in this final state are the lowest, but they still contribute ∼18% to the total number of events. A significance of 23.27σ is achieved at an integrated luminosity of 3000 fb^{-1} for BP1. In BP2, the $\tilde{R}_2^{+2/3}$ pair production leads to the largest number of events, as a result of the ∼40% probability of $2j$ + OSD. A lesser number of events are observed in the case of $X_{1,2}^{-1/3}$ individually, while showing a combined ∼55% probability of achieving the FS1 in this BP2. The signal significance for the total number of events is found to be 16.21σ at 3000 fb^{-1} of integrated luminosity. In BP3, as a consequence of ∼100% probability of $2j$ + OSD, the numbers for $\tilde{R}_2^{+2/3}$ dominate this final state. The tiny probabilities of ∼8% for $X_1^{-1/3}$ and ∼3% for $X_2^{-1/3}$ leads to very small event numbers in this final state, constituting ∼7% of the total number. However, the signal significance of 19.34σ is promising for this BP3 as well, with an integrated luminosity of 3000 fb^{-1}. Moving to a higher E_{CM} of 27 TeV, similar patterns are observed for the event numbers in the case of each pair-produced leptoquark as those at 14 TeV. Here, at an integrated luminosity of 1000 fb^{-1}, $\geq 59\sigma$ significances are achieved for all three BPs. Finally, at the highest E_{CM} of 100 TeV, ∼158σ or larger significances are obtained at 100 fb^{-1} of integrated luminosity. From Table XII, it is also clear that in this final state the model can be probed with 5σ significance at < 300 fb^{-1} luminosities for 14 TeV, with the lowest being ∼138 fb^{-1} for BP1. With this observation, one can predict a 5σ probe of the BP1 scenario in this FS1 at the end of the current LHC run 3 of 13.6 TeV center-of-mass energy, with the projected integrated luminosity of ∼400 fb^{-1} [189]. For 27 and 100 TeV, the 5σ probe of this model can be achieved with very early stage data.

3. 2 jets + 0 c/τ jets + OSD

While in FS1 we considered a final state with c jets to facilitate higher numbers for $X_{1,2}^{-1/3}$, in this final state (FS2) given by Eq. (4.3), we veto out events with c jets instead of b jets, keeping in mind that $2b$ jets + OSD can be obtained

from $\tilde{R}_2^{+2/3}$ for BP1 and BP2. The number of signal and background events are tabulated in Table XIII, for the three leptoquarks across the benchmark scenarios, at the center-of-mass energies of 14, 27, and 100 TeV at the LHC/FCC. The SM decay chain of $t\bar{t} \to 2b + 2W \to 2\,b\,\text{jets} + \text{OSD}$ ensures a very dominant background contribution from $t\bar{t}$. Concerning the signal, we see near-equivalent contributions from $\tilde{R}_2^{+2/3}, X_{1,2}^{-1/3}$ in BP1, while in both BP2 and BP3, $\tilde{R}_2^{+2/3}$ dominates. At 14 TeV for BP1, we observe an enhancement of events for $\tilde{R}_2^{+2/3}$ compared to FS1, as a result of bringing the b jets into the picture, as suggested by Table XI. However, $X_{1,2}^{-1/3}$ shows similar numbers as FS1, indifferent to the consideration of b or c jets alike, owing to no decay mode of $X_{1,2}^{-1/3}$ directly leading to a b/c jet and a charged lepton (Table II). In BP2 and BP3, the numbers are dominated by $\tilde{R}_2^{+2/3}$, both due to the consideration of b jets and the rejection of c jets, similarly predicted by Table XI. The number of events for $X_1^{-1/3}$ and $X_2^{-1/3}$ together contribute ∼23% for BP2, and ∼3% for BP3. The combined number of events for the three leptoquarks lead to the feasibility of probing the model with 22.02σ, 11.81σ, and 15.25σ, respectively for BP1, BP2 and BP3, at the 14 TeV LHC with an integrated luminosity of 3000 fb^{-1}. Moving to a higher center-of-mass energy of 27 TeV, the signal significances are even more improved, with $75.73\sigma, 46.91\sigma$, and 57.67σ, for BP1–BP3 respectively, considering an integrated luminosity of 1000 fb^{-1}. The simulation at 100 TeV FCC improves these numbers even more drastically, where at 100 fb^{-1} luminosity, the model can be probed with significances of $189.77\sigma, 132.17\sigma$, and 139.59σ, respectively for the three BPs. Similar to FS1, a 5σ probe of the model can be achieved at the 14 TeV LHC with < 550 fb^{-1} luminosity for each benchmark point. Similar to the case of FS1, the numbers predict a possible 5σ probe of BP1 at the end of LHC run 3 of $E_{CM} = 13.6$ TeV, with ∼400 fb^{-1} of projected integrated luminosity. In the higher energies of 27 and 100 TeV, this 5σ probe is predicted to be obtained with much earlier data.

Thus, the final state topologies described by Eqs. (4.2) and (4.3) contain the potential of achieving 5σ signatures for the $\tilde{R}_2$ and S_1 extension of the SM, with rich phenomenology encompassing the three chosen benchmark scenarios. These final states are considered in such a way that, for each benchmark point, some entries of the Yukawa couplings contribute towards obtaining them for each pair of $\tilde{R}_2^{+2/3}$ and $X_{1,2}^{-1/3}$ that are produced at the LHC/FCC. While FS1 and FS2 here are probes of this Beyond the Standard Model (BSM) extension as a whole, we also intend to study the possibilities of distinguishing between the pure doublet

TABLE XIII. The number of signal and background events for the topology FS2 in Eq. (4.3) for the pair production of the three leptoquarks at the LHC/FCC, across the three benchmark points. The numbers are presented for center-of-mass energies of 14, 27, and 100 TeV, with integrated luminosities of 3000, 1000 and 100 fb^{-1} for each E_{CM}, respectively. The signal significances and the required luminosities for a 5σ signal strength $\mathcal{L}_{5\sigma}$ are also presented.

		$\geq$2 jets + 0 c/τ-jets + OSD + $p_T^{\ell^+,\ell^-} \geq$300.0 GeV							
		Signal			Backgrounds				
E_{CM} (TeV)	Pair produced leptoquark	BP1	BP2	BP3	$t\bar{t}$	VV	VVV	$t\bar{t}V$	tVV
14	$\tilde{R}_2^{+2/3}$	329.61	329.86	567.93					
	$X_1^{-1/3}$	396.86	49.73	12.04	662.83	195.65	20.77	5.06	2.29
	$X_2^{-1/3}$	215.19	48.47	5.00					
Total		941.66	428.06	584.97			886.60		
Significance		22.02σ	11.81σ	15.25σ					
$\mathcal{L}_{5\sigma}(\text{fb}^{-1})$		154.63	538.10	322.53					
27	$\tilde{R}_2^{+2/3}$	2634.68	2625.18	4599.96					
	$X_1^{-1/3}$	2874.61	459.54	109.77	1498.83	456.20	70.59	14.64	4.97
	$X_2^{-1/3}$	1826.10	405.47	46.81					
Total		7335.39	3490.19	4756.54			2045.24		
Significance		75.73σ	46.91σ	57.67σ					
$\mathcal{L}_{5\sigma}(\text{fb}^{-1})$		4.36	11.36	7.51					
100	$\tilde{R}_2^{+2/3}$	15089.50	15384.40	21893.60					
	$X_1^{-1/3}$	13632.90	2871.55	759.10	3113.17	769.85	138.90	33.61	11.84
	$X_2^{-1/3}$	10979.60	2616.28	288.68					
Total		39702.00	20872.20	22941.38			4067.37		
Significance		189.77σ	132.17σ	139.59σ					
$\mathcal{L}_{5\sigma}(\text{fb}^{-1})$		0.07	0.14	0.13					

$\tilde{R}_2^{+2/3}$ and the mixed states $X_{1,2}^{-1/3}$, as well as between the mixed states $X_1^{-1/3}$ and $X_2^{-1/3}$ themselves. In the next sections, we will discuss these possibilities one by one.

V. DISTINGUISHING BETWEEN $\tilde{R}_2^{+2/3}$ AND $X_{1,2}^{-1/3}$

For the three chosen benchmark scenarios in this work, the three leptoquarks $\tilde{R}_2^{+2/3}$, $X_1^{-1/3}$ and $X_2^{-1/3}$ are nearly degenerate, with masses $\approx$1.5 TeV. However, $\tilde{R}_2^{+2/3}$ being a pure doublet and $X_{1,2}^{-1/3}$ being mixed states have different combinations of the Yukawa couplings dictating their dominant decay modes. In particular, $\tilde{R}_2^{+2/3}$ only couples to a down-type quark and a charged lepton via $\mathcal{Y}_2$, which can be seen by expanding the model Lagrangian in Eq. (2.1). On the other hand, $X_{1,2}^{-1/3}$ can couple to an up-type quark and a charged lepton, or a down-type quark and a neutrino, via different combinations of $\mathcal{Y}_1^{L,R}$ and $\mathcal{Y}_2$. Nonetheless, both the pure doublet and the mixed states can lead to final states with nontagged light jets and a pair of oppositely signed leptons that are not identified as electrons or muons. Now, a distinction can be made between $\tilde{R}_2^{+2/3}$ and $X_{1,2}^{-1/3}$ by virtue of their charge difference, by studying the charge distribution of the jets emanating from them, similar to the work done in Refs. [155,156,190–192]. However, in this article, we wish to look at a few final state topologies that will give us event numbers that are heavily dominated by either $\tilde{R}_2^{+2/3}$ or $X_{1,2}^{-1/3}$. While we witnessed such a dominance for $\tilde{R}_2^{+2/3}$ pair-production events in the case of BP3 for the FS2 as discussed in Sec. IV C, it is important to note that the FS2 events still contained direct consequences of the Yukawa couplings for $X_{1,2}^{-1/3}$. In this section, we will look at topologies facilitated by the Yukawa couplings for either the pure doublet or the mixed states, so that any small contamination from either is a resultant of the ISR/FSR activities. For example, a final state of two b-jets + 2OSe is only allowed for $\tilde{R}_2^{+2/3}$ by the coupling $\mathcal{Y}_2$ in BP1 and BP2, but there can be slight contaminations from $X_{1,2}^{-1/3}$ due to b jets arising from ISR/FSR effects. With this discussion in mind, as well as the information provided by Table XI, we can now look for four such final states with which we will try to discern $\tilde{R}_2^{+2/3}$ and $X_{1,2}^{-1/3}$.

A. 2 b-jets + 2 OSe

In both BP1 and BP2, the pure doublet leptoquark $\tilde{R}_2^{+2/3}$, when pair produced, can lead to a final state of two b-tagged jets and two oppositely signed electrons (Table XI), from the $\tilde{R}_2^{+2/3} \to be^+$ decay happening via the $(\mathcal{Y}_2)^{31}$ element. Similar to Sec. IV C, we can put a cut of $p_T^{e^+,e^-} \geq 300.0$ GeV, to remove a large portion of the SM background for a cleaner signal. The complete final state is given as follows:

$$\textbf{FS3}: n_{b\text{-jet}} \geq 2 \quad \text{and} \quad n_{e^+} = n_{e^-} = 1 \quad \text{and} \quad n_{\text{light}/c/\tau\text{-jets}} = 0 \quad \text{and} \quad p_T^{e^+,e^-} \geq 300.0 \text{ GeV}. \tag{5.1}$$

Table XIV displays the signal and background event numbers for this final state, simulated from pair productions of each leptoquark under consideration at the LHC/FCC with three center-of-mass energies of 14, 27 and 100 TeV. The SM background is very small in this case and it mainly comes from $t\bar{t}$, contributing to the b-jet pair. The first thing we notice here is that, for BP3, we get a negligible number of events due to the absence of this final state there, as shown in Table XI. However, BP1 and BP2 give us very interesting results. At 14 TeV in BP1, a large majority of the events pertain to $\tilde{R}_2^{+2/3}$, with a $\sim$3% contamination from $X_{1,2}^{-1/3}$ combined. For BP2, only $\tilde{R}_2^{+2/3}$ contributes to this final state, and zero contamination is observed from the mixed states. This is due to the absence of dielectron final states for $X_{1,2}^{-1/3}$ pair production in the BP2 scenario. The FS3 in these benchmark points are shown to be probed with significances of 7.16σ and 5.46σ, respectively, for BP1 and BP2, with 3000 fb^{-1} of integrated luminosity. This distinction of $\tilde{R}_2^{+2/3}$ from $X_{1,2}^{-1/3}$ can be observed with 5σ significance, at integrated luminosities of 1464.17 and 2516.68 fb^{-1}, which are within the limits of the HL-LHC. The observed SM background here is very minimal due to the stringent cuts on the jet and lepton identities, with most of it being contributed by $t\bar{t}$. The same $\tilde{R}_2^{+2/3}$ dominance is observed at $E_{CM} = 27$ TeV, with the signal significance now increasing to 22.52σ in BP1, and 17.76σ in BP2, with an integrated luminosity of 1000 fb^{-1}. At 100 TeV center-of-mass energy, this distinction can be observed with a significance of 54.48σ in BP1, and 44.31σ in BP2, with 100 fb^{-1} luminosity. The required 5σ significance can be obtained with < 80 fb^{-1} luminosity at 27 TeV, while at 100 TeV it comes down to < 2 fb^{-1}, for both BP1 and BP2. The FS3 topology can thus act as a probe of the Yukawa coupling $(\mathcal{Y}_2)^{31}$ itself, while being able to distinguish the $\tilde{R}_2^{+2/3}$ pair production signal from $X_{1,2}^{-1/3}$.

B. 1 light jet + 1 c jet + 2 OSμ

In the case of BP2, Table XI predicts a significant probability of dimuons in the final states for $X_{1,2}^{-1/3}$ pair production, while for $\tilde{R}_2^{+2/3}$ this probability is seen to be zero. On the other hand, BP3 sees a 100% probability of having oppositely signed muon pairs in the final states from $\tilde{R}_2^{+2/3}$ pair production, with a negligibly small probability in the case of $X_{1,2}^{-1/3}$. Considering the $\sim$20% effective branching for a final state involving one light and one c-tagged jet alongside a pair of oppositely signed muons (OSμ) from $X_{1,2}^{-1/3}$ at BP2, we decide to study the events of

TABLE XIV. The number of signal and background events for the topology FS3 in Eq. (5.1) for the pair production of the three leptoquarks at the LHC/FCC, across the three benchmark points. The numbers are presented for center-of-mass energies of 14, 27, and 100 TeV, with integrated luminosities of 3000, 1000 and 100 fb^{-1} for each E_{CM}, respectively. The signal significances and the required luminosities for a 5σ signal strength $\mathcal{L}_{5\sigma}$ are also presented.

		$\geq 2\,b$-jets $+\,0\,\text{light}/c/\tau$-jets $+\,2\,\text{OS}e + p_T^{e^+,e^-} \geq 300.0$ GeV							
		Signal			Backgrounds				
E_{CM} (TeV)	Pair produced leptoquark	BP1	BP2	BP3	$t\bar{t}$	VV	VVV	$t\bar{t}V$	tVV
14	$\tilde{R}_2^{+2/3}$	72.11	49.79	0.03					
	$X_1^{-1/3}$	1.44	0.0	0.0	33.39	0.0	0.0	0.0	0.0
	$X_2^{-1/3}$	0.71	0.0	0.0					
Total		74.26	49.79	0.03					
Significance		7.16σ	5.46σ	0.005σ					
$\mathcal{L}_{5\sigma}$(fb^{-1})		1464.17	2516.68	$\gg 3000$					
27	$\tilde{R}_2^{+2/3}$	578.60	400.79	0.15					
	$X_1^{-1/3}$	13.08	0.0	0.0	106.78	0.0	0.0	1.71	0.0
	$X_2^{-1/3}$	7.37	0.0	0.0					
Total		599.05	400.79	0.15			108.49		
Significance		22.52σ	17.76σ	0.01σ					
$\mathcal{L}_{5\sigma}$(fb^{-1})		49.29	79.26	$\gg 1000$					
100	$\tilde{R}_2^{+2/3}$	3123.94	2274.82	0.88					
	$X_1^{-1/3}$	88.35	0.0	0.0	355.07	2.12	0.0	3.36	0.0
	$X_2^{-1/3}$	81.14	0.0	0.0					
Total		3293.43	2274.82	0.88			360.55		
Significance		54.48σ	44.31σ	0.05σ					
$\mathcal{L}_{5\sigma}$(fb^{-1})		0.84	1.27	$\gg 100$					

the following final state as a means of distinguishing between the pure doublet and the mixed states:

$$\textbf{FS4}: \; n_{\text{light jet}} \geq 1 \quad \text{and} \quad n_{c\text{-jet}} \geq 1 \quad \text{and} \quad n_{\mu^+} = n_{\mu^-} = 1 \quad \text{and} \quad n_{b/\tau\text{-jets}} = 0 \quad \text{and} \quad p_T^{\mu^+,\mu^-} \geq 300.0 \text{ GeV}. \tag{5.2}$$

In Table XV, the signal and background event numbers are presented for the pair production of the three leptoquarks at 14, 27 and 100 TeV LHC/FCC energies, pertaining to the final state FS4 described in Eq. (5.2). The applied cuts and vetoes keep the SM background contribution minimal. This time, the insignificant event numbers are seen for BP1 owing to the unavailability of OSμs in any final state, as seen from Table XI. As a consequence of the ∼32% branching ratios of both $X_{1,2}^{-1/3}$ in $c\mu$ and $u\mu$ decay modes, as well as the zero probability of OSμ pairs from $\tilde{R}_2^{+2/3}$, the event numbers for BP2 are very similar for $X_1^{-1/3}$ and $X_2^{-1/3}$, while zero events are observed from $\tilde{R}_2^{+2/3}$ pair production. The situation gets reversed in BP3, where the total number of events is dominated by $\tilde{R}_2^{+2/3}$, with ∼4% contamination from $X_{1,2}^{-1/3}$ pair productions combined. Here, even though the exact final state of FS4 is not predicted for $\tilde{R}_2^{+2/3}$ in Table XI, the 100% probability of obtaining OSμ pairs lead to a significant number of events here, with the additional required c jet provided by ISR/FSR effects. Thus, in the BP2 scenario, events in this FS4 topology pertain only to the mixed leptoquark states $X_{1,2}^{-1/3}$, governed by the Yukawa coupling combinations $(\mathcal{Y}_1^R)_{12} + (\tilde{\mathcal{Y}}_1^L)_{12}$ and $(\mathcal{Y}_1^R)_{23} + (\tilde{\mathcal{Y}}_1^L)_{23}$ (Table III). However, in the BP3 scenario, FS3 is a probe of the pure doublet state $\tilde{R}_2^{+2/3}$, where the required jet and dimuon final state is provided by the Yukawa couplings $(\mathcal{Y}_2)_{12}$ and $(\mathcal{Y}_2)_{22}$ (Table IV). These distinctions are achieved with significances of 13.22σ for BP2 and 6.57σ for BP3, at the 14 TeV LHC with an integrated luminosity of 3000 fb^{-1}. A 5σ probe can be achieved with HL-LHC luminosities of 429.06 and 1733.16 fb^{-1}, respectively for BP2 ad BP3. At the higher center-of-mass energy of 27 TeV, the same discerning signatures are obtained with 40.18σ and 20.87σ significances, respectively for BP2 and BP3, with 1000 fb^{-1} luminosity. At 100 TeV center-of-mass energy and 100 fb^{-1} luminosity, these significances increase to 104.8σ for BP2, and 55.63σ for BP3. In both of these higher center-of-mass energies, early data can provide the required 5σ significance (<60 fb^{-1} for 27 TeV, <1 fb^{-1} for 100 TeV). Thus, unlike FS3, this topology can point

TABLE XV. The number of signal and background events for the topology FS4 in Eq. (5.2) for the pair production of the three leptoquarks at the LHC/FCC, across the three benchmark points. The numbers are presented for center-of-mass energies of 14, 27, and 100 TeV, with integrated luminosities of 3000, 1000 and 100 fb^{-1} for each E_{CM}, respectively. The signal significances and the required luminosities for a 5σ signal strength $\mathcal{L}_{5\sigma}$ are also presented.

			$\geq$1 light jets + $\geq$1c-jets + 0b/τ-jets + 2 OSμ + $p_T^{\mu^+,\mu^-}\geq$300.0 GeV						
			Signal			Backgrounds			
E_{CM} (TeV)	BP1	Pair produced leptoquark	BP2	BP3	$t\bar{t}$	VV	VVV	$t\bar{t}V$	tVV
14	$\tilde{R}_2^{+2/3}$	0.0	0.0	48.76					
	$X_1^{-1/3}$	0.0	94.35	1.26	5.13	3.25	0.0	0.0	0.0
	$X_2^{-1/3}$	0.01	88.46	0.44					
Total		0.01	182.81	50.46			8.38		
Significance		0.003σ	13.22σ	6.57σ					
$\mathcal{L}_{5\sigma}$(fb^{-1})		$\gg$3000	429.06	1733.16					
27	$\tilde{R}_2^{+2/3}$	0.0	0.0	473.73					
	$X_1^{-1/3}$	0.06	875.87	13.53	38.13	13.89	9.43	0.0	1.63
	$X_2^{-1/3}$	0.11	800.11	4.41					
Total		0.17	1675.98	491.67			63.08		
Significance		0.02σ	40.18σ	20.87σ					
$\mathcal{L}_{5\sigma}$(fb^{-1})		$\gg$1000	15.48	57.37					
100	$\tilde{R}_2^{+2/3}$	0.77	0.0	3069.96					
	$X_1^{-1/3}$	0.89	5883.05	109.21	63.40	46.65	22.21	0.0	4.44
	$X_2^{-1/3}$	1.54	5235.57	47.59					
Total		3.2	11118.62	3226.76			136.70		
Significance		0.27σ	104.80σ	55.63σ					
$\mathcal{L}_{5\sigma}$(fb^{-1})		$\gg$100	0.23	0.81					

towards either the mixed states or the pure doublet state, considering the benchmark scenario.

C. 1 light jet + 1 b jet + 2 OSe

In the case of both BP1 and BP2, Table XI shows us the strong presence of a final state containing one light jet, one b jet and a pair of oppositely signed electrons (OSe), which come from the $\tilde{R}_2^{+2/3}$ pair production, but are absent in the case of $X_{1,2}^{-1/3}$. This presents us with another opportunity of distinguishing $\tilde{R}_2^{+2/3}$ from $X_{1,2}^{-1/3}$ from pair production events. The complete final state topology is given as follows:

$$\textbf{FS5}:\ n_{\text{light jet}} \geq 1 \quad \text{and} \quad n_{b\text{-jet}} \geq 1 \quad \text{and} \quad n_{e^+} = n_{e^-} = 1 \quad \text{and} \quad n_{c/\tau\text{-jets}} = 0 \quad \text{and} \quad p_T^{e^+,e^-} \geq 300.0 \text{ GeV}. \tag{5.3}$$

Table XVI depicts the number of signal and background events for FS5, coming from the pair production of all three leptoquarks at 14, 27 and 100 TeV center-of-mass energies at the LHC/FCC. As expected, for BP3 the signal event numbers are insignificant. BP1 shows a heavy dominance of $\tilde{R}_2^{+2/3}$ events, while a tiny ~4% combined contamination from $X_{1,2}^{-1/3}$ pair production is observed, due to the high probability of dielectron events (Table XI). In BP2 however, $\tilde{R}_2^{+2/3}$ pair production is responsible for all the events in this topology, as no dielectron final states are facilitated by the $\mathcal{Y}_1^{L,R}$ for $X_{1,2}^{-1/3}$ in this scenario. The pattern remains consistent through all three center-of-mass energies, with small backgrounds mostly arising from $t\bar{t}$, owing to more b-jet-tagged events. Similar to all the previous final states, very promising signal significances are obtained at each center-of-mass energy for both BP1 and BP2. At 14 TeV, the pure doublet $\tilde{R}_2^{+2/3}$ stands apart from the mixed states with a significance of 9.77σ for BP1, and 6.97σ for BP2, with a luminosity of 3000 fb^{-1}. The required 5σ significance is achieved at < 1600 fb^{-1} luminosity for both BP1 and BP2 in this case. At 27 TeV energy with 1000 fb^{-1} luminosity, these signals are enhanced to 33.82σ for BP1 and 25.11σ for BP2, requiring < 40 fb^{-1} luminosities to probe them up to 5σ significance. Finally, the 100 TeV FCC simulation at 100 fb^{-1} luminosity gives us 89.87σ significance for BP1 and 70.61σ in the case of BP2. Here, <1 fb^{-1} luminosity is enough to probe this discerning signature with a 5σ significance. In both BP1 and BP2, the FS5 topology mainly arises from the combination of doublet Yukawa couplings $(\mathcal{Y}_2)_{21} + (\mathcal{Y}_2)_{31}$ (Table IV).

TABLE XVI. The number of signal and background events for the topology FS5 in Eq. (5.3) for the pair production of the three leptoquarks at the LHC/FCC, across the three benchmark points. The numbers are presented for center-of-mass energies of 14, 27, and 100 TeV, with integrated luminosities of 3000, 1000 and 100 fb^{-1} for each E_{CM}, respectively. The signal significances and the required luminosities for a 5σ signal strength $\mathcal{L}_{5\sigma}$ are also presented.

		$\geq$1 light jets + $\geq$1 b-jets + 0 c/τ-jets + 2 OSe + $p_T^{e^+,e^-} \geq$300.0 GeV							
		Signal			Backgrounds				
E_{CM} (TeV)	Pair produced leptoquark	BP1	BP2	BP3	$t\bar{t}$	VV	VVV	$t\bar{t}V$	tVV
14	$\tilde{R}_2^{+2/3}$	184.31	122.80	0.06					
	$X_1^{-1/3}$	3.44	0.0	0.0	184.98	0.0	1.97	0.0	0.45
	$X_2^{-1/3}$	2.05	0.0	0.0					
Total		189.80	122.80	0.06			187.40		
Significance		9.77σ	6.97σ	0.005σ					
$\mathcal{L}_{5\sigma}$(fb^{-1})		785.32	1542.82	$\gg$3000					
27	$\tilde{R}_2^{+2/3}$	1515.37	1001.96	0.3					
	$X_1^{-1/3}$	34.54	0.0	0.0	556.82	16.20	5.03	3.60	3.61
	$X_2^{-1/3}$	23.48	0.0	0.0					
Total		1573.39	1001.96	0.3			585.26		
Significance		33.82σ	25.11σ	0.01σ					
$\mathcal{L}_{5\sigma}$(fb^{-1})		21.85	39.65	$\gg$1000					
100	$\tilde{R}_2^{+2/3}$	8600.97	5913.14	0.88					
	$X_1^{-1/3}$	239.17	0.0	0.0	1014.47	42.40	20.37	15.12	7.39
	$X_2^{-1/3}$	217.16	0.0	0.78					
Total		9057.30	5913.14	1.66			1099.75		
Significance		89.87σ	70.61σ	0.05σ					
$\mathcal{L}_{5\sigma}$(fb^{-1})		0.31	0.50	$\gg$100					

D. 2 light jets + $\not{p}_T$

The neutrinos that emerge from any SM or BSM particle decay, remain "invisible" at the LHC detectors. Due to the conservation of total p_T, these invisible neutrinos account for some missing transverse momentum $\not{p}_T$. From our model Lagrangian it is observed that the component of $\tilde{R}_2$ with electric charge $-1/3$, as well as $S_1^{-1/3}$, can couple to a down-type quark and a neutrino via $\mathcal{Y}_2$ and $\mathcal{Y}_1^L$ couplings, respectively. Especially for BP2 and BP3, Table XI shows us the probabilities of obtaining a pair of light jets along with some $\not{p}_T$ that is carried by the neutrinos directly emanating from $X_{1,2}^{-1/3}$ leptoquarks. Having a heavy ($\sim$1.5 TeV) particle as the mother, the p_T of these neutrinos are expected to be large, similar to the case with the leptons as seen in Fig. 6.

In Fig. 7, we show the missing transverse momentum distributions in a final state with two light jets and $\not{p}_T$, for

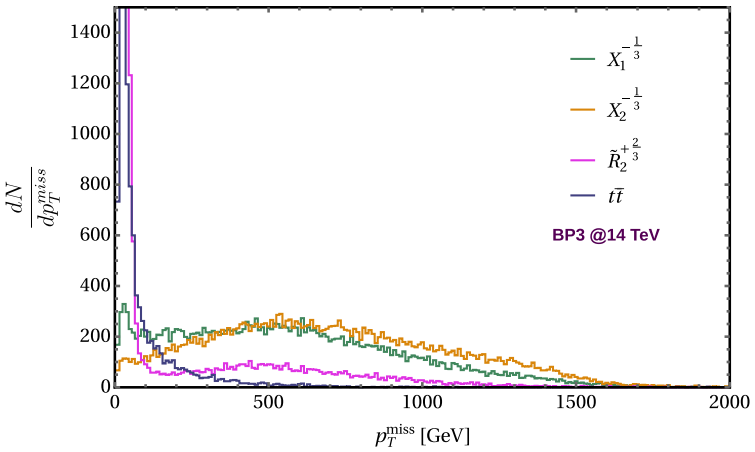

FIG. 7. Distributions of $\not{p}_T$ in a $2j + \not{p}_T$ final state, from pair production of the three leptoquarks at 14 TeV LHC, for BP1. The same distribution is also shown for the $t\bar{t}$ SM background.

the pair productions of $\tilde{R}_2^{+2/3}$ (pink), $X_1^{-1/3}$ (green), and $X_2^{-1/3}$ (yellow), for BP3 at the 14 TeV LHC. The same distribution arising from the SM background of $t\bar{t}$ (dominant) is also shown (dark blue). As expected, a wide peak is observed around ∼600 GeV for both $X_{1,2}^{-1/3}$ leptoquark cases, accounting for the neutrinos that they decay into. However, owing to the lesser probability of this state for $X_2^{-1/3}$ (Table XI), another sharp peak is seen at around ∼50 GeV. This peak signifies the neutrinos that come from other SM processes, such as decays of the τ from $X_{1,2}^{-1/3} \to u\tau^-$ modes. In the case of $X_1^{-1/3}$, this earlier peak is negligible due to higher probability of obtaining $2j + \not{p}_T$. The distributions for $\tilde{R}_2^{+2/3}$ almost mimic that of $t\bar{t}$, but with a longer tail, with the only significant peak occurring at around ∼50 GeV. This allows us to put an advanced cut of $\not{p}_T \geq 500$ GeV in order to eliminate more of the SM background contribution, leading us to the final state:

$$\textbf{FS6}: n_{\text{light jet}} \geq 2 \quad \text{and} \quad n_{\text{lep}} = 0 \quad \text{and} \quad n_{b/c/\tau\text{-jets}} = 0 \quad \text{and} \quad \not{p}_T \geq 500.0 \text{ GeV}. \tag{5.4}$$

In Table XVII we present the number of events in the FS6 topology for the leptoquark pair production signals as well as the SM backgrounds, at 14, 27 and 100 TeV center-of-mass energies of the LHC/FCC. While in each benchmark scenario the majority of events are seen to be coming from $X_{1,2}^{-1/3}$, the $\tilde{R}_2^{+2/3}$ pair production events account for about 11% in BP1, and 10% in BP2, which are not very negligible. This happens due to the lesser or no probability of obtaining a $2j + \not{p}_T$ final state from $X_{1,2}^{-1/3}$ in BP1 and BP2, as seen in Table XI. However, the situation is interesting in the case of BP3. Owing to the higher probabilities of $2j + \not{p}_T$ for $X_{1,2}^{-1/3}$, the events pertaining to $\tilde{R}_2^{+2/3}$ contribute < 5% to the FS6 for BP3. Again, dominated by the comparatively large doublet Yukawa coupling of $(\mathcal{Y}_2)_{12} \approx 0.876$, the numbers for $X_2^{-1/3}$ (containing ∼66% doublet) are almost twice those for $X_1^{-1/3}$. This approximate 1:2 ratio is maintained by $X_1^{-1/3}$ and $X_2^{-1/3}$, irrespective of the center-of-mass energy. Considering the tiny contamination from $\tilde{R}_2^{+2/3}$ pair production events, for BP3 this final state topology can act as a distinguisher in favor of the mixed leptoquarks $X_{1,2}^{-1/3}$, against the pure doublet. At the 14 TeV LHC, this probe is achieved with a significance of 7.82σ, for 3000 fb^{-1} luminosity. The 5σ signal strength is achievable at 1224.22 fb^{-1} luminosity. Moving to the higher center-of-mass energy of 27 TeV with a luminosity of 1000 fb^{-1}, the signal significance increases to 27.52σ, while at

TABLE XVII. The number of signal and background events for the topology FS6 in Eq. (5.4) for the pair production of the three leptoquarks at the LHC/FCC, across the three benchmark points. The numbers are presented for center-of-mass energies of 14, 27, and 100 TeV, with integrated luminosities of 3000, 1000 and 100 fb^{-1} for each E_{CM}, respectively. The signal significances and the required luminosities for a 5σ signal strength $\mathcal{L}_{5\sigma}$ are also presented.

		≥2 light jets + 0 leptons + $0b/c/\tau$-jets + $\not{p}_T$ ≥ 500.0 GeV							
		Signal			Backgrounds				
E_{CM} (TeV)	Pair produced leptoquark	BP1	BP2	BP3	$t\bar{t}$	VV	VVV	$t\bar{t}V$	tVV
14	$\tilde{R}_2^{+2/3}$	3.04	5.31	8.16					
	$X_1^{-1/3}$	20.05	28.89	51.70	236.35	45.65	5.93	7.63	0.23
	$X_2^{-1/3}$	11.91	31.53	108.83					
Total		35.00	65.73	168.69			295.80		
Significance		1.92σ	3.46σ	7.82σ					
$\mathcal{L}_{5\sigma}$(fb^{-1})		≫3000	≫3000	1224.22					
27	$\tilde{R}_2^{+2/3}$	26.85	47.78	67.63					
	$X_1^{-1/3}$	158.23	303.62	519.61	1666.64	272.10	57.14	31.00	3.61
	$X_2^{-1/3}$	116.03	302.95	1088.45					
Total		301.11	654.35	1675.69			2030.49		
Significance		6.23σ	12.62σ	27.52σ					
$\mathcal{L}_{5\sigma}$(fb^{-1})		642.90	156.76	32.99					
100	$\tilde{R}_2^{+2/3}$	209.45	329.19	399.46					
	$X_1^{-1/3}$	900.47	2011.79	3688.64	5202.36	816.50	142.61	157.95	59.20
	$X_2^{-1/3}$	770.51	2114.71	7315.32					
Total		1880.43	4455.69	11403.42			6378.63		
Significance		20.69σ	42.81σ	85.51σ					
$\mathcal{L}_{5\sigma}$(fb^{-1})		5.83	1.36	0.34					

100 TeV FCC with 100 fb^{-1} of luminosity, the FS6 shows a 85.51σ strength of signal. In both of these higher-energy LHC/FCC, the 5σ probe is shown to be obtained with very early data.

The study of these four final state event numbers can thus provide a way to discern the singlet and doublet leptoquarks in different benchmark scenarios of the Yukawa coupling structures. The difference in decay modes between singlet and doublet states as shown in Table XI can also help us reconstruct the invariant mass of these leptoquarks, which we will discuss in detail in the next subsection.

E. Invariant mass distributions

One peculiar characteristic of a leptoquark, by definition, is that it can decay to a quark and a lepton, after production. The quark eventually leads to a hadronic jet at the LHC, and the invariant mass of the jet-lepton pair can be used to reconstruct the leptoquark resonance. However, the resolutions of high-momentum jets and leptons are reported to be low, hampering a high-precision reconstruction of the leptoquark mass peaks for the time being. The CMS detector currently reports ∼5% resolution for $p_T^{\rm jet} \geq$ 200.0 GeV [193]. While a resolution of 3 GeV is achieved for muons at the Z-boson peak, the resolutions for muons in general with $p_T^{\mu} \geq 200.0$ GeV may vary from ∼3% to ∼5% [194]. This leads to the current reports of CMS searches for leptoquarks using 100 GeV invariant mass bins for a jet-lepton pair [172,173]. Nevertheless, in this work we are using a more optimistic scenario where the bin widths for such distributions are taken as 10 GeV.

Across our three benchmark scenarios, the leptoquark masses remain the same, with the values of 1.502, 1.499, and 1.506 TeV, respectively for $\tilde{R}_2^{+2/3}$, $X_1^{-1/3}$ and $X_2^{-1/3}$. Such nearly degenerate mass resonances are very challenging to distinguish in the same final state, due to the high resolution that is required. However, each of the BPs provide us with a final state that is different for the pure state $\tilde{R}_2^{+2/3}$ with respect to the mixed states $X_{1,2}^{-1/3}$ as seen in Table XI, and we will be focusing on these final states in this subsection. For BP1, we can look for the invariant mass distribution of one b jet and one electron, in a final state of two b jets and a pair of OSe, without any light, c- or τ-tagged jets, in which we expect to obtain a clean peak for $\tilde{R}_2^{+2/3}$, considering the SM backgrounds as well as the combined events from $\tilde{R}_2^{+2/3}$ and $X_{1,2}^{-1/3}$ pair production. For BP2, a distinct peak for $\tilde{R}_2^{+2/3}$ is expected from two light jets and two OSe in the final state, whereas for BP3 we will be looking at a final state of two light jets and two OSμ. It is important to note that, for each of these cases, different combinations of jet-lepton are possible, and only the correct combination will lead to the mass peak. Additionally, tagging the exact charge of the lepton can help us obtain the peak specific to $\tilde{R}_2^{+2/3}$ or $\tilde{R}_2^{-2/3}$. In each case, a cut of $p_T^{\ell} \geq 300.0$ GeV is imposed, in order to filter out the majority of backgrounds.

In Fig. 8 we display the invariant mass distributions from the channels discussed above, simulated at the 27 TeV LHC with 1000 fb^{-1} of integrated luminosity. In each panel, the dark red distributions show the combined events for $\tilde{R}_2^{+2/3}$ and $X_{1,2}^{-1/3}$ pair production, summed with the total SM background events in that final state. The dotted distributions show the events for each individual pair production of leptoquarks $\tilde{R}_2^{+2/3}$ (pink), $X_1^{-1/3}$ (green), and $X_2^{-1/3}$ (yellow), along with the SM background (dark blue). Figure 8(a) shows the invariant mass distribution of one e^- and one b-tagged jet (M_{e^-b}) in a 2b jet +2 OSe final state, obtained from BP1. The absence of b-jet events in the final states of $X_{1,2}^{-1/3}$ in this scenario, as well as the demand of high-p_T electrons, almost nullify the contributions from $X_{1,2}^{-1/3}$ and the SM backgrounds, and the peak obtained at ∼1500 GeV can be pinpointed to the pure doublet $\tilde{R}_2^{-2/3}$. Similarly, in Fig. 8(b), the invariant mass of one e^+ and one b jet (M_{e^+b}) gives the peak for $\tilde{R}_2^{+2/3}$. In Fig. 8(c) we observe the invariant mass distribution of one light jet and one e^- (M_{e^-j}), for BP2. Here, the lack of dielectron final states in $X_{1,2}^{-1/3}$ pair production leads to almost zero contamination from the mixed states, and the peak at ∼1500 GeV again consists almost entirely of events pointing to $\tilde{R}_2^{-2/3}$. One again, demanding e^+ instead of e^- in Fig. 8(d) leads to a clean peak for $\tilde{R}_2^{+2/3}$. A similar story is observed in Fig. 8(e), where the invariant mass distribution of one μ^- and one light jet (M_{μ^-j}) for BP3 leads to a clean peak at ∼1500 GeV for $\tilde{R}_2^{-2/3}$, with next to zero contribution from $X_{1,2}^{-1/3}$ and the SM backgrounds, while the M_{μ^+j} peak consists almost entirely of events from $\tilde{R}_2^{+2/3}$, as seen in Fig. 8(f).

To summarize, the benchmark point-specific invariant mass distribution of one lepton and one jet can lead to a distinct resonance peak of $\tilde{R}_2^{+2/3}$ and its antiparticle, untainted by the SM backgrounds as well as events from $X_{1,2}^{-1/3}$ pair production. This provides us with another way of distinguishing the pure doublet leptoquark from the mixed states. However, the conversation changes when it comes to distinguishing between the mixed states themselves, which will be detailed in the following section.

VI. DISTINGUISHING BETWEEN $X_1^{-1/3}$ AND $X_2^{-1/3}$

In Sec. V, we performed an analysis of final states observed in the pair production events of $\tilde{R}_2^{+2/3}$, $X_1^{-1/3}$, and $X_2^{-1/3}$, through which we can distinguish the pure state $\tilde{R}_2^{+2/3}$ from the mixed states $X_{1,2}^{-1/3}$. We also successfully obtained $\tilde{R}_2^{+2/3}$ resonance peaks from different jet-lepton invariant mass distributions, for each of the three

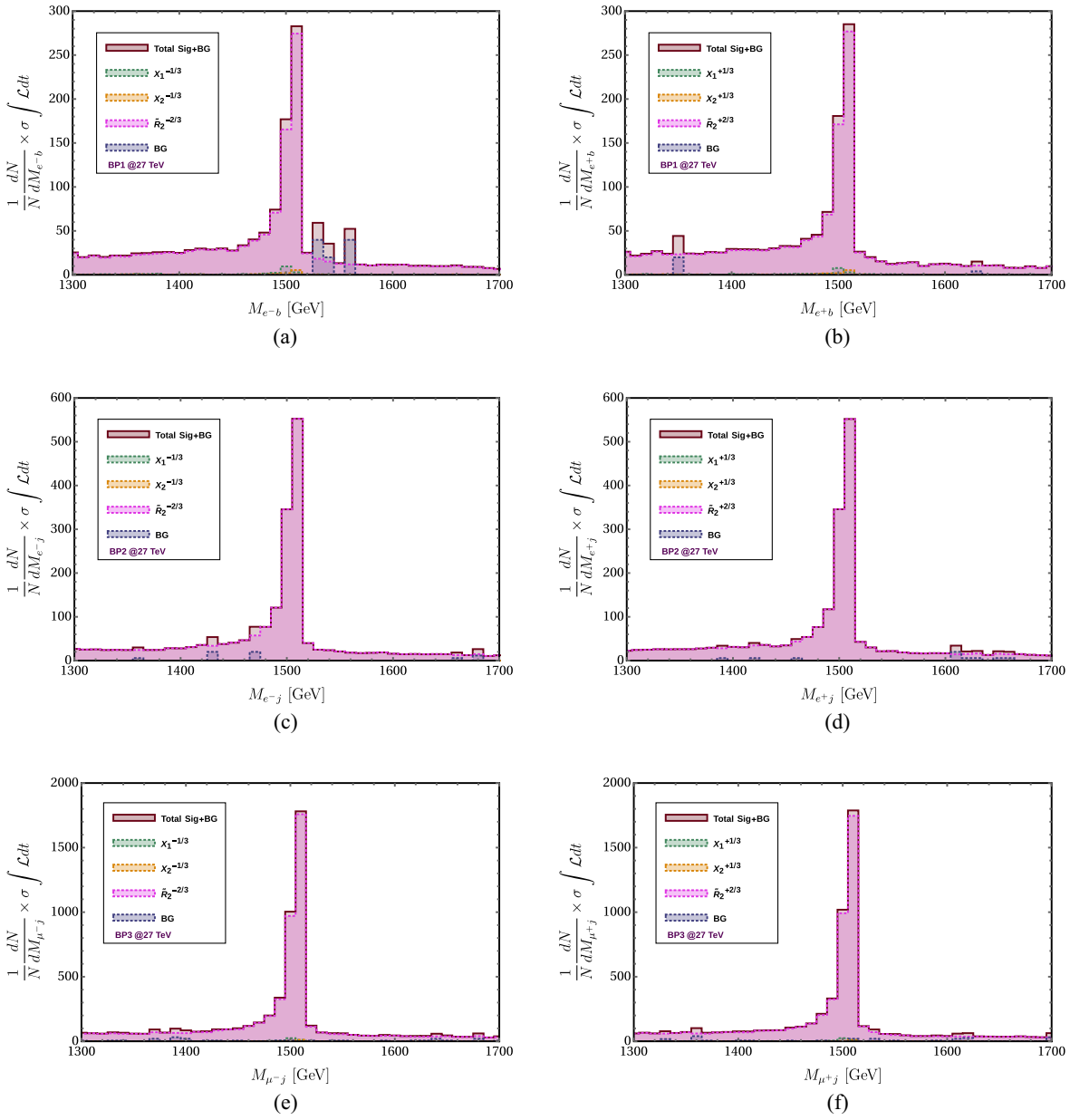

FIG. 8. Invariant mass distributions of (a) e^-b and (b) e^+b in BP1, (c) e^-j and (d) e^+j in BP2, (e) μ^-j and (f) μ^+j in BP3, from the pair production of leptoquarks at the 27 TeV LHC.

benchmark points in consideration. The difference in their electromagnetic charge makes it relatively easier to obtain discerning signatures that favor either $\tilde{R}_2^{+2/3}$ or $X_{1,2}^{-1/3}$, even though they are nearly degenerate in the mass spectrum. However, when it comes to distinguishing between the mixed states $X_1^{-1/3}$ and $X_2^{-1/3}$, in the context of our benchmark points, it becomes more challenging. Especially in BP1 and BP2, where both $X_1^{-1/3}$ and $X_2^{-1/3}$ have almost the same branching ratios and probable final states from their pair production (Table XI), it becomes increasingly difficult to obtain a signature where either one of them has a negligible contribution compared to the other.

In BP3, due to the difference in branching ratios, we observed an event ratio of $\approx 1:2$ in the final state FS6, described in Table XVII. Regardless, for the purpose of distinguishing, the number differences need to be even larger. The large mixing angle $\theta_{LQ} = -0.618$ radians leads to ~66.5% singlet and ~33.5% doublet content in $X_1^{-1/3}$, with the ratios reversed for $X_2^{-1/3}$, as discussed in Sec. III. Therefore, even with comparably large entries in $\mathcal{Y}_2$ and $\mathcal{Y}_1^{L,R}$, there is no significant dominance observed for any one of them in BP3, for either of the two mixed leptoquarks. In the following subsections, we will be discussing some approaches that are viable in this regard.

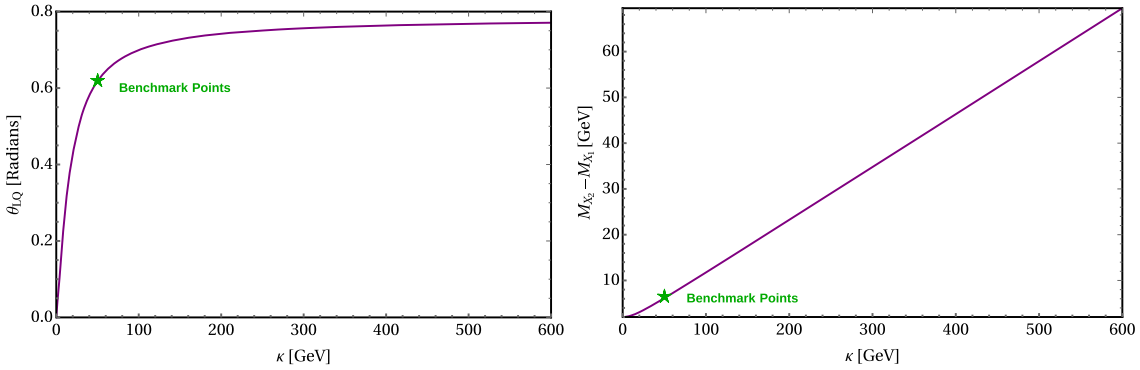

(a) (b)

FIG. 9. Variation of (a) leptoquark mixing angle and (b) $X_{1,2}$ mass splitting with respect to κ. The green star corresponds to the benchmark of $\kappa = 50$ GeV.

A. The leptoquark mixing angle

The mixing between the $Q = 1/3$ component of the doublet leptoquark $\tilde{R}_2$ and the singlet leptoquark S_1 influences the discernability of $X_1^{-1/3}$ and $X_2^{-1/3}$ significantly. As seen from Eq. (2.4), for fixed values of m_1, m_2, α_1, α_2 and α_3, the value of θ_{LQ} depends only upon the value of the trilinear coupling κ. Again, Eq. (2.5) shows how κ affects the masses of $X_{1,2}^{-1/3}$. Therefore, with the change in κ, the mass splitting $\Delta M_{21} = M_2 - M_1$ also changes, which again affects the distinguishability further.

Figure 9 illustrates how changes in κ affects the mixing angle and the mass splitting, as discussed above. The value of θ_{LQ} has a fast increase up to $\kappa = 100$ GeV, and then it slows down, becoming almost constant over a wide range of κ, as portrayed by Fig. 9(a). The mass splitting however follows a linear trend, shown in Fig. 9(b). In both of these plots, our benchmark value of $\kappa = 50$ GeV is shown with the green stars. For this value of κ, we have $|\theta_{LQ}| \approx 0.618$, and $\Delta M_{21} \approx 7$ GeV. If we can determine the mixing angle from a production process at the LHC/FCC, then we are at an advantage when it comes to distinguishing between $X_{1,2}^{-1/3}$. Theoretically, the difference in doublet content of these two mixed states allows one such production process, which we will discuss in the next subsection.

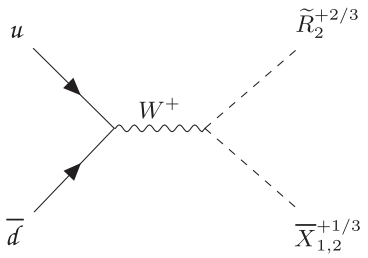

FIG. 10. Associated production of $\tilde{R}_2^{+2/3}$ with $\bar{X}_{1,2}^{+1/3}$ via an s-channel W^+ boson at the LHC.

B. Distinguishing $X_{1,2}^{-1/3}$ from asymmetric production

While our previous discussion dealt with the phenomenology of leptoquark pair production, in this subsection we present a possibility of distinguishing between the mixed leptoquark states with the help of the asymmetric production process of $q\overline{q'} \to \tilde{R}_2^{+2/3}\bar{X}_{1,2}^{+1/3}$. This production is facilitated by the s-channel exchange of a $W^{\pm}$ gauge boson, as shown in Fig. 10. As only the doublet components of $X_{1,2}^{-1/3}$ couple to the $W^{\pm}$ boson, the parameter κ and subsequently the mixing angle θ_{LQ} plays a role in these production cross sections.

Figures 11(a)–11(c) show the κ dependence of the cross sections at energies of 14, 27 and 100 TeV, respectively, where the red line corresponds to $\tilde{R}_2^{+2/3}\bar{X}_1^{+1/3}$ and the blue line to $\tilde{R}_2^{+2/3}\bar{X}_2^{+1/3}$ production processes. We see that, when $\kappa = 0$ GeV, the cross section involving $X_1^{-1/3}$ remains zero, as there is zero doublet component in this. With the increase in κ, the $X_1^{-1/3}$ cross section increases while the $X_2^{-1/3}$ cross section comes down. Figures 11(d)–11(f) show the same variation of the two production cross sections, with respect to the leptoquark mixing angle θ_{LQ}. From both of these plots, we observe that even though $M_2 > M_1$, the production cross section of $\tilde{R}_2^{+2/3}\bar{X}_2^{+1/3}$ stays higher than that of $\tilde{R}_2^{+2/3}\bar{X}_1^{+1/3}$ up to a certain value of κ or θ_{LQ}. The point at which these two cross sections overlap is different for different center-of-mass energies. Before reaching the intersection point, the difference in cross section is dominated by the amount of doublet/singlet percentage in the leptoquark. At the intersection point, the effect of the mass gap cancels out that of θ_{LQ}. As the mass splitting increases, the availability of phase space becomes the dominant factor, and so after that point the production process involving the lighter of the two mixed leptoquarks has higher cross section than that of the heavier leptoquark. An important observation here is that the point of intersection corresponds to a smaller κ (or θ_{LQ}) for a lesser E_{CM}.

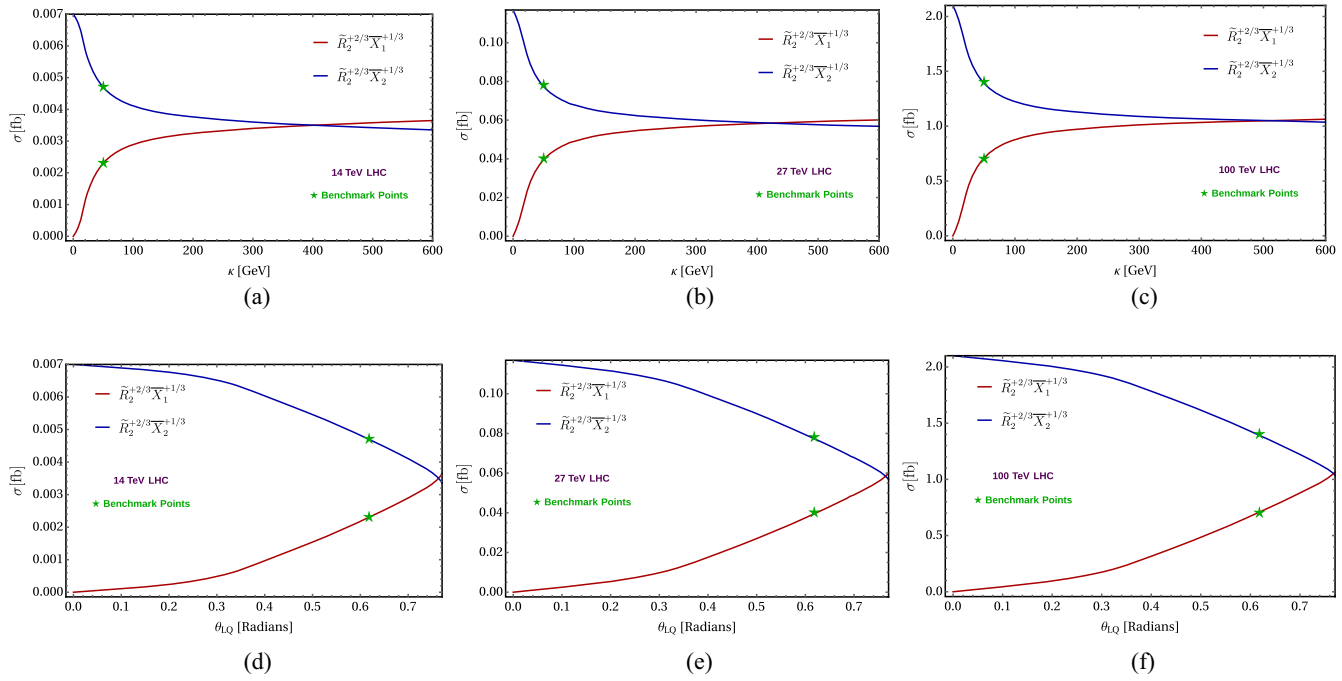

FIG. 11. The variation of $\sigma_{\tilde{R}_2^{+2/3}\bar{X}_{1,2}^{+1/3}}$ with respect to κ [Figs. 11(a)–11(c)], and with respect to θ_{LQ} [Figs. 11(d)–11(f)] for three different E_{CM}s of 14, 27 and 100 TeV. In each plot, the red line corresponds to X_1 and the blue line to X_2. The green star shows our choice of $\kappa = 50$ GeV and $\theta_{LQ} = 0.617998$ for the BPs.

The crossover happens at κ (θ_{LQ}) values of ∼400 GeV (0.7636 rad), ∼420 GeV (0.7647 rad) and ∼500 GeV (0.7680 rad), for center-of-mass energies of 14, 27 and 100 TeV, respectively. These threshold values increase with E_{CM} due to the enhancement in availability of the phase space with E_{CM}. Therefore, at higher energies, the effect of mixing angle can be observed for a longer range compared to lower energies. Within this range, the measured values of cross sections at the same final state can point towards the leptoquark with either more singlet content, or more doublet.

In Table XVIII the LO cross sections for the production of $\tilde{R}_2^{+2/3}\bar{X}_1^{+1/3}$ and $\tilde{R}_2^{+2/3}\bar{X}_2^{+1/3}$ are presented for three center-of-mass energies of 14, 27, and 100 TeV, at the LHC/FCC. These cross sections are independent of the choice of Yukawa couplings, and so they remain the same in each case for all three BPs. Naturally, as $X_2^{-1/3}$ contain twice as much doublet percentage as $X_1^{-1/3}$ (∼66.5% and ∼33.5%), the value of $\sigma_{\tilde{R}_2^{+2/3}\bar{X}_2^{+1/3}}$ is almost 2 times that of $\sigma_{\tilde{R}_2^{+2/3}\bar{X}_1^{+1/3}}$, in each center-of-mass energy. This difference in cross sections between $X_1^{-1/3}$ and $X_2^{-1/3}$ can act as a probe of the mixing angle θ_{LQ} itself. The cross sections are, however, very low as the masses of the leptoquarks are high and a massive gauge boson mediates the process. Such cross sections will not lead us to a number of observed events that is large enough to draw conclusive remarks from it, from an experimental perspective. At the HL-LHC limit of 3000 fb^{-1} luminosity, the production processes at 14 TeV will lead to a total of less than fifteen observed events, for both $X_1^{-1/3}$ and $X_2^{-1/3}$. At 27 TeV, with 1000 fb^{-1} luminosity, the observed events still remain low, with less than 80 events for both leptoquarks. At the 100 TeV FCC, the cross sections predict the observation of less than 110 events for $X_1^{-1/3}$ and $X_2^{-1/3}$, with 100 fb^{-1} of integrated luminosity. These observed event numbers are too small for a proper analysis, and with advanced kinematic and phase space cuts, they will decrease even

TABLE XVIII. Associated production cross sections of $\tilde{R}_2^{+2/3}\bar{X}_{1,2}^{+1/3}$ at LO via s-channel W^+-boson exchange for all three BPs, and three different E_{CM}s of 14, 27 and 100 TeV at the LHC.

	$pp \to W^{\pm} \to LQ_1\overline{LQ_2}$ at different E_{CM}s					
	$\sigma_{\tilde{R}_2^{+2/3}\bar{X}_1^{+1/3}}$ (fb)			$\sigma_{\tilde{R}_2^{+2/3}\bar{X}_2^{+1/3}}$ (fb)		
BPs	14 TeV	27 TeV	100 TeV	14 TeV	27 TeV	100 TeV
BP 1–3	0.002	0.039	0.71	0.004	0.078	1.40

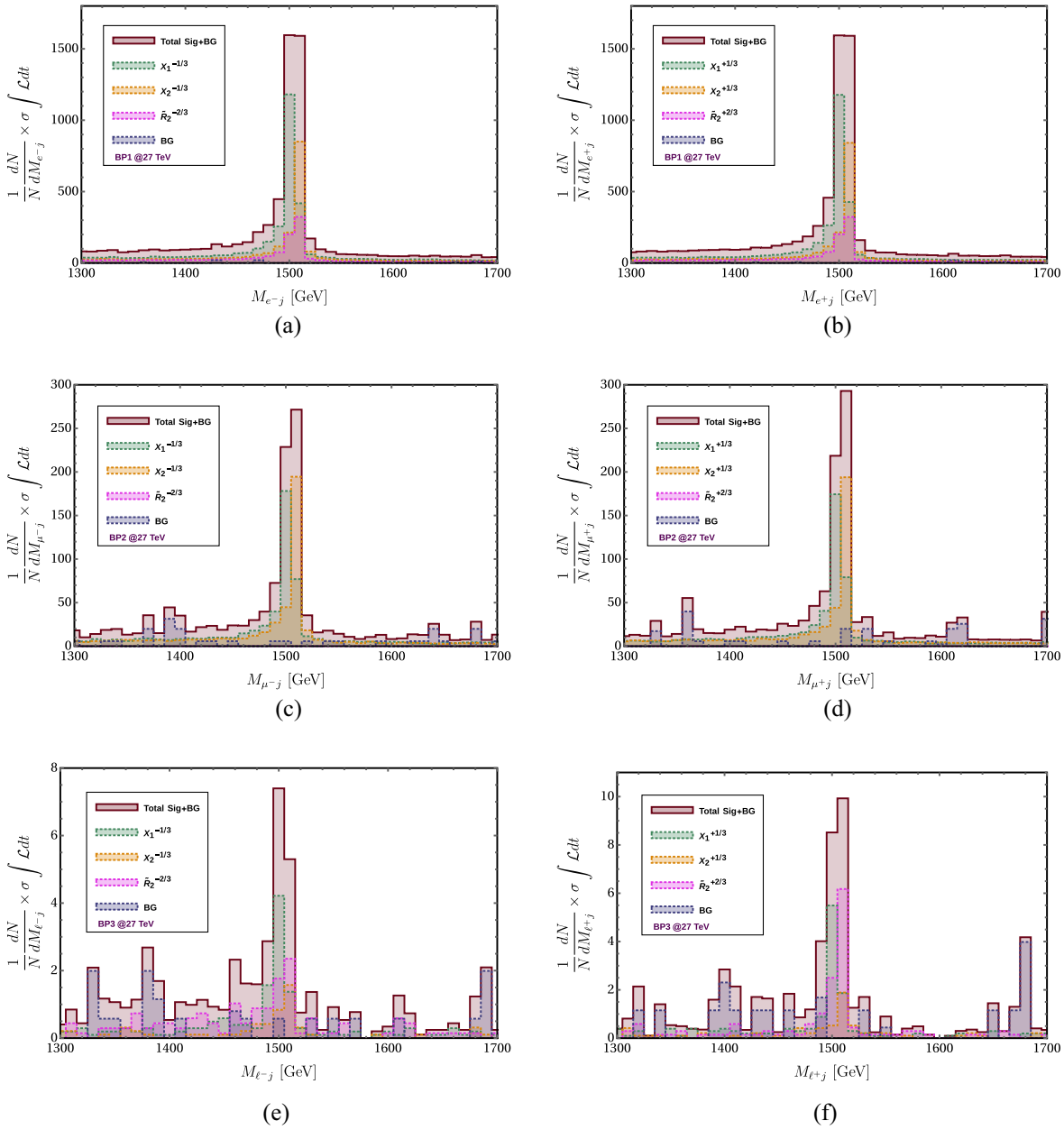

FIG. 12. Invariant mass distributions of (a) e^-j and (b) e^+j in BP1, (c) μ^-j and (d) μ^+j in BP2, (e) ℓ^-j and (f) ℓ^+j in BP3, from the pair production of leptoquarks at the 27 TeV LHC.

further. Thus, while being theoretically sound, this production mode is not experimentally viable, in probing the leptoquark mixing angle, as well as in distinguishing between $X_1^{-1/3}$ and $X_2^{-1/3}$, and one needs to wait for higher energy and higher integrated luminosity.

C. Distinguishing $X_{1,2}^{-1/3}$ from pair production

The experimental impracticality of the asymmetric pair production process in discerning between the mixed leptoquarks leads us back to the discussion of the pair production processes. In the preceding analysis we have observed that, for the chosen set of mass, mixing and Yukawa couplings, obtaining a clear signature that pinpoints towards either $X_1^{-1/3}$ or $X_2^{-1/3}$ is extremely challenging from the pair production processes. In the following subsections, a few possible approaches for resolving such a near-degenerate pair of mixed leptoquarks are presented.

1. Invariant mass distribution

In Sec. V E, we have already discussed the challenges when it comes to resolving reconstructed invariant mass peaks of leptoquark resonances. As our benchmark points allow different final states for $\tilde{R}_2^{+2/3}$ and $X_{1,2}^{-1/3}$, we could perform reconstructions of the $\tilde{R}_2^{+2/3}$ leptoquark from

different final states involving two jets and two leptons, with negligible contaminations from the SM backgrounds as well as from $X_{1,2}^{-1/3}$, as shown in Fig. 8. The situation becomes tricky when we want to do the same for $X_1^{-1/3}$ and $X_2^{-1/3}$ individually. In our BPs, the mass splitting between these two states is just 7 GeV, which requires high-precision resolution of the reconstructed peaks. However, as mentioned in Sec. V E, this precision cannot be obtained with the current LHC resolutions of high-momentum jets and leptons that need to be used for the reconstruction. To properly resolve between two states separated by a mass of 7 GeV, we would require ∼2 GeV of bin width, which is far too optimistic in the current context. Nevertheless, just like for $\tilde{R}_2^{+2/3}$, we present some invariant mass distributions at the 27 TeV LHC with 10 GeV bin widths, to explain the situation better.

Figure 12 shows a few invariant mass distributions of jet-lepton pairs that can reconstruct the mixed leptoquark mass peaks. In each case, the dark red distribution signifies the total signal events of the three leptoquark pair production processes, combined with the SM background. The dotted lines represent the individual contributions from $\tilde{R}_2^{+2/3}$ (pink), $X_1^{-1/3}$ (green), and $X_2^{-1/3}$ (yellow), and the SM background (dark blue). In Fig. 12(a) we show the invariant mass distribution of one light jet and one e^- (M_{e^-j}), obtained in a $2j+2$ OSe final state in the case of BP1. Here, as expected, events from both $X_1^{-1/3}$ and $X_2^{-1/3}$ contribute to the total observed peak at ∼1.5 TeV, with a small contribution also coming from $\tilde{R}_2^{-2/3}$. This obtained peak cannot pinpoint to either $X_1^{-1/3}$ or $X_2^{-1/3}$. Figure 12(b) shows the distribution of M_{e^+j}, with dominant contribution to the peaks from $X_{1,2}^{+1/3}$. Again, Fig. 12(c) displays the invariant mass distribution of one light jet and one μ^- (M_{μ^-j}) in a $2j+2$ OSμ final state, pertaining to the leptoquark pair productions in BP2. Here, the contribution of $\tilde{R}_2^{-2/3}$ is nullified due to the absence of muons in its decays. However, similar to BP1, the peak has dominant contributions from both $X_1^{-1/3}$ and $X_2^{-1/3}$, which cannot be resolved. The same outcome is seen from the M_{μ^+j} distribution in Fig. 12(d), the peak of which has contributions from both $X_{1,2}^{+1/3}$. For BP3, the probabilities of obtaining a final state with two jets and two leptons is very rare for $X_{1,2}^{-1/3}$ pair production. We evaluate the invariant mass of one light jet and one electron or muon (denoted as $\ell^\pm$) from the $2j+1e^\pm+1\mu^\mp$ final state as described in Table XI. The distributions of M_{ℓ^-j} and M_{ℓ^+j} are presented in Figs. 12(e) and 12(f), respectively. Here, the number of events are very low for each leptoquark, and owing to the high abundance of events with two light jets and at least one muon, the $\tilde{R}_2^{+2/3}$ contribution is even more than that of $X_2^{-1/3}$.

If one wishes to utilize this invariant mass peak in distinguishing $X_1^{-1/3}$ and $X_2^{-1/3}$, one possible way is to have an increase in the mass splitting. This can be done by setting the bare mass terms m_1 and m_2 in the Lagrangian in Eq. (2.1) to be unequal, unlike in our consideration where $m_1 = m_2 = 1500$ GeV. A difference in m_1 and m_2 can also lead to a much smaller value of θ_{LQ}, thus increasing the singlet and doublet percentages in $X_1^{-1/3}$ and $X_2^{-1/3}$, respectively. The phenomenology will then change for such a parameter set, and it will also affect the neutrino data and the LFV branching fractions under consideration. In this work we are not considering such a nondegenerate scenario.

Nevertheless, with the rapid enhancement in machine learning algorithms, the resolution of jets and leptons are becoming more precise at the LHC. The top quark mass, for example, is now measured with a precision of < 1 GeV [195], while the resolution for muons at the Z-mass peak is < 3 GeV [194]. The SM Higgs boson mass has also been measured with a < 1 GeV resolution [196,197]. We need to wait for such dedicated high-resolution analysis being available for high-mass leptoquark studies, so that the invariant mass peaks of $X_{1,2}^{-1/3}$ are distinguishable.

2. Final state modes

Considering for the time being that the value of κ is negligibly small or zero, the mixing between the leptoquarks also vanishes, as seen in Fig. 9. Then, the decays of $\tilde{R}_2^{+2/3}$ and $\tilde{R}_2^{-1/3}$ are purely governed by $\mathcal{Y}_2$, while the $S_1^{-1/3}$ leptoquark decays only via $\mathcal{Y}_1^{L,R}$, as seen from Eq. (2.1). This allows $S_1^{-1/3}$ to decay into an up-type quark and a charged lepton, while $\tilde{R}_2^{-1/3}$ can decay into a down-type quark and a neutrino. Meanwhile, $\tilde{R}_2^{+2/3}$ can decay only to a down-type quark and a charged lepton. Hints of such a case are already found in Table II, where, due to the inertness of the small $\mathcal{Y}_2$, the decays of $X_1^{-1/3}$ and $X_2^{-1/3}$ happen into ue^- and $c\tau^-$ for a combined 87% of the time, while $\tilde{R}_2^{+2/3}$ decays 100% into be^+ and se^+.

Assuming all three leptoquark states to be pure, irrespective of the Yukawa coupling structures, the generic final states that can be obtained from their pair production are as follows:

$$\tilde{R}_2^{+2/3}\tilde{R}_2^{-2/3} \to 2\text{-jets} + \text{OSD}; \quad \tilde{R}_2^{-1/3}\tilde{R}_2^{+1/3} \to 2\text{-jets} + \not{p}_T; \tag{6.1}$$

$$S_1^{-1/3}S_1^{+1/3} \to 2\text{-jets} + \text{OSD} \quad \text{and} \quad 2\text{-jets} + \not{p}_T. \tag{6.2}$$

We can expect an abundance of dijet and dilepton events in the case of the singlet pair production, while the $Q = -1/3$ doublet component will lead to dijet events with some large missing transverse momenta. For smaller values of θ_{LQ}, an

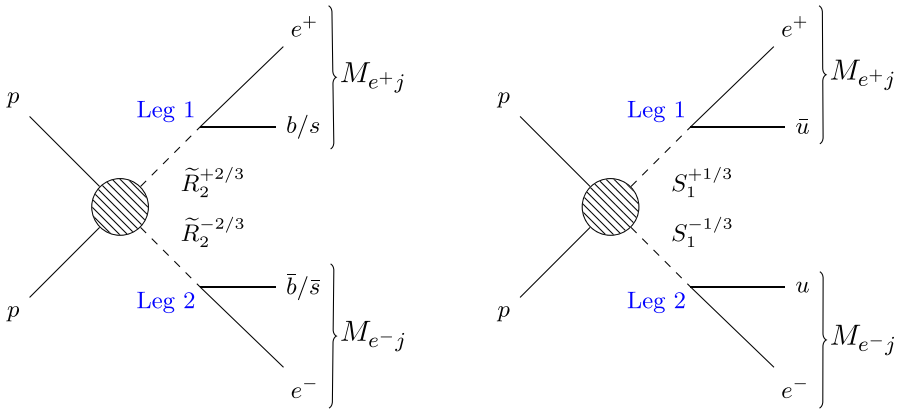

FIG. 13. Cartoon diagrams in the context of jet charge analysis, for pair production of $\tilde{R}_2^{+2/3}$ (left) and $S_1^{-1/3}$ (right) in case of BP1.

analysis of events in either of these final states can lead to the heavy domination of $X_1^{-1/3}$ or $X_2^{-1/3}$ pair production. Even with cases like BP3 where the entries of $\mathcal{Y}_1^{L,R}$ and $\mathcal{Y}_2$ are of comparable order, distinct signatures can be achieved if the points are chosen with a tiny mixing angle. Again, each one of $\tilde{R}_2^{-1/3}$ and $S_1^{1/3}$ emanates differently charged quarks for a fixed lepton charge. This can also be crucial for differentiating between $X_1^{-1/3}$ and $X_2^{-1/3}$, which we will discuss in the next subsection.

3. Jet charge

In our analysis of segregating between $\tilde{R}_2^{+2/3}$ and $X_{1,2}^{-1/3}$ in Sec. V, the utility of jet charge reconstruction was mentioned. Continuing our assumption of negligible mixing where $X_1^{-1/3}$ and $X_2^{-1/3}$ are essentially $S_1^{-1/3}$ and $\tilde{R}_2^{-1/3}$, we can tag a lepton with its identity and charge specified, and then identify the jet that is produced with it from the same leg of the pair production diagram [155,156,190–192]. The correct jet can be identified by demanding the jet-lepton invariant mass to be within a ± 5 GeV window of the leptoquark resonance, with the help of the discussion in Secs. VI C 1 and V E. After identifying the jet, we can study the charge distribution of it, to determine whether it originates from an up-type quark (coming from $\tilde{R}_2^{+2/3}$) or a down-type quark (coming from $S_1^{-1/3}$), which can eventually lead us to correctly identifying the responsible leptoquark, as shown in Fig. 13. For example, in the case of BP1, the Fig. 13 shows the 2-jet + 2OSe final states obtainable from $\tilde{R}_2^{+2/3}$ and $S_1^{-1/3}$ pair production. Table II shows how from the pair production of $\tilde{R}_2^{+2/3}$, tagging an e^- automatically ensures the jet coming from leg 2 to be of $\bar{s}$ or $\bar{b}$ flavor, in the correct invariant mass pairing. Whereas, in the case of $S_1^{-1/3}$, the tagged e^- from the invariant mass pair will point to a u-flavored jet from leg 2. Considering a scenario of negligible θ_{LQ}, $\tilde{R}_2^{-1/3}$ will not even have that required electron at the first place. Hence, from the combined analysis of pair production of the three leptoquarks, we can observe two different Gaussian distributions, which may overlap for some part. Now, if $\tilde{R}_2$ did not exist in the model, we would be seeing only one distribution pertaining to the u-flavored jets. Similarly, absence of S_1 will show us the $\bar{s}$- or $\bar{b}$-flavored distribution. As the mixing angle increases, the number of events in the $X_1^{-1/3}$ jet charge distribution decreases, due to the enhancement of $\tilde{R}_2^{-1/3}$ percentage in it. This deviation from the ideal case can be utilized to estimate the mixing angle itself.

VII. CONCLUSION

In this work we generate Majorana neutrino masses via a one-loop Weinberg operator involving $\tilde{R}_2$ and S_1 leptoquarks, which are in $SU(2)$ doublet and singlet representations, respectively. We further investigate the model parameter space which can satisfy the neutrino mixing angles, anomalous magnetic moment of the muon and electron, as well as various experimental bounds coming from lepton flavor violating processes. Once setting up with these we study various final state topologies in probing different mass eigenstates involving $\tilde{R}_2$ and S_1 at the LHC/FCC.

Due to the presence of a trilinear coupling κ, the component of $\tilde{R}_2$ with charge $1/3$ mixes with S_1 through an angle θ_{LQ} to give us two mass eigenstates $X_{1,2}^{-1/3}$, while the $\tilde{R}_2^{+2/3}$ mass eigenstate remains a pure doublet. Thus, we have three physically observable leptoquark states from this model, on which we perform a study at the LHC/FCC. For the purpose of the collider simulations, we choose three sets of Yukawa couplings in three benchmark points with different phenomenological implications. The entries of these couplings are chosen in such a way that they agree to the neutrino mass and oscillation data, the $g-2$ of muon and electron, as well as the experimental bounds on various LFV processes, simultaneously. In each benchmark point, a nearly degenerate mass spectrum is considered for the leptoquarks, with $M_{\tilde{R}_2^{+2/3}} = 1.502\,\text{TeV}$, $M_{X_1^{-1/3}} = 1.499\,\text{TeV}$, and $M_{X_2^{-1/3}} = 1.506$ TeV.

We begin our study with the pair production of each of the three physical leptoquark states. The pair production is mostly dominated by the QCD processes of gluon-gluon fusion and s-channel gluon exchange from quark fusions. However, based on the choice of Yukawa couplings, the t-channel lepton exchange diagrams can also contribute to the pair production cross section. The three sets of Yukawa couplings in the three benchmark points show us different phenomenology in each case. The analysis is performed at center-of-mass energies of 14, 27 and 100 TeV to simulate the present and future LHC/FCC environments.

The first step of the collider analysis (Sec. IV C) involves obtaining signatures to probe the model at the LHC/FCC with two different final state topologies: 2 light/c-jets + OSD (FS1), and 2 light/b-jets + OSD (FS2). In both final states, 5σ probes of the model are achieved across the three benchmark points at the 14 TeV LHC, with < 540 fb^{-1} integrated luminosity in each case (Tables XII and XIII). With higher energies of 27 and 100 TeV, the 5σ significance is shown to be obtained with much earlier data.

Next, in Sec. V, signatures to distinguish between the pure doublet $\tilde{R}_2^{+2/3}$ and the mixed states $X_{1,2}^{-1/3}$ are explored from the pair production processes. Four different final state topologies are identified (FS3-FS6), with which we can perform such a distinction. Depending on the benchmark points, the obtained signal events in these states are dominated by either $\tilde{R}_2^{+2/3}$ or $X_{1,2}^{-1/3}$. In each final state, discerning signatures are obtained for at least one BP, with 5σ probes being possible within $\sim$2500 fb^{-1} luminosity limit at the 14 TeV LHC. Once again, at higher center-of-mass energies, these signatures are obtained at much less luminosities of < 80 fb^{-1} at 27 TeV, and <1.5 fb^{-1} at 100 TeV. The $\tilde{R}_2^{+2/3}$ leptoquark is also shown to be distinctly reconstructed from the invariant mass distributions of one jet and one lepton, with the identities varying for different BPs, with negligible contamination from $X_{1,2}^{-1/3}$ and SM background events.

Lastly, in Sec. VI, we discuss the challenges and possibilities of discerning $X_1^{-1/3}$ from $X_2^{-1/3}$. Their small mass splitting of $\sim$7 GeV, same electric charge, and large mixing angle of $|\theta_{LQ}| = 0.618$ radians lead to complications in obtaining final states that are dominated heavily by either one of them. The mixing angle plays a part in the asymmetric production mode of $q\bar{q}' \to \tilde{R}_2^{+2/3}\bar{X}_{1,2}^{+1/3}$ via s-channel $W^{\pm}$-boson exchange, which can, in theory, allow us to probe θ_{LQ} and act as a way of distinguishing. However, small values of cross sections make this probe impractical from the current experimental perspective. Moving back to pair production, the tiny mass gap remains unresolved, even with an optimistic bin width of 10 GeV, and we need to wait for the advancement in the precision of high-momentum jet and lepton resolution. For a smaller mixing angle, the stark difference in the singlet and doublet decay modes can help us obtain distinguishing signatures. A jet charge analysis of these modes can also reflect the effect of the mixing, and act as a probe of $X_1^{-1/3}$ or $X_2^{-1/3}$.

ACKNOWLEDGMENTS

S. P. sincerely thanks the Council of Scientific and Industrial Research (CSIR), India, for funding his research (File No. 09/1001(0082)/2020-EMR-I). S. P. also acknowledges Chandrima Sen for some valuable discussion regarding PYTHIA. P. B. and A. K. acknowledge SERB CORE Grant No. CRG/2018/004971 and MATRICS Grant No. MTR/2020/000668 for the financial support. A. K. also acknowledges the partial support by MCIN/AEI/10.13039/501100011033 Grant No. PID2020–114473 GB-I00, and Grant No. PROMETEO/2021/071 (Generalitat Valenciana). K. G. and Avnish acknowledge SERB Core Research Grant No. CRG/2019/006831. S. P. and P. B. also acknowledge SERB Karyashala titled "Data and Machine Learning at the Large Hadron Collider" (DML@LHC-2022), Grant No. AV/KAR/2022/0167.

[1] S. Weinberg, Baryon and Lepton Nonconserving Processes, Phys. Rev. Lett. **43**, 1566 (1979).
[2] P. Minkowski, $\mu \to e\gamma$ at a rate of one out of 10^9 muon decays?, Phys. Lett. **67B**, 421 (1977).
[3] T. Yanagida, Horizontal gauge symmetry and masses of neutrinos, Conf. Proc. C **7902131**, 95 (1979).
[4] M. Gell-Mann, P. Ramond, and R. Slansky, Complex spinors and unified theories, Conf. Proc. C **790927**, 315 (1979).
[5] R. N. Mohapatra and G. Senjanovic, Neutrino Mass and Spontaneous Parity Nonconservation, Phys. Rev. Lett. **44**, 912 (1980).
[6] M. Magg and C. Wetterich, Neutrino mass problem and gauge hierarchy, Phys. Lett. **94B**, 61 (1980).
[7] J. Schechter and J. W. F. Valle, Neutrino masses in SU(2) × U(1) theories, Phys. Rev. D **22**, 2227 (1980).
[8] C. Wetterich, Neutrino masses and the scale of B-L violation, Nucl. Phys. **B187**, 343 (1981).
[9] G. Lazarides, Q. Shafi, and C. Wetterich, Proton lifetime and fermion masses in an SO(10) model, Nucl. Phys. **B181**, 287 (1981).
[10] R. N. Mohapatra and G. Senjanovic, Neutrino masses and mixings in gauge models with spontaneous parity violation, Phys. Rev. D **23**, 165 (1981).

[11] T. P. Cheng and L.-F. Li, Neutrino masses, mixings and oscillations in SU(2) × U(1) models of electroweak interactions, Phys. Rev. D **22**, 2860 (1980).

[12] S. Ashanujjaman, K. Ghosh, and K. Huitu, Type-II see-saw: Searching the LHC elusive low-mass triplet-like Higgses at e^-e^+ colliders, Phys. Rev. D **106**, 075028 (2022).

[13] S. Ashanujjaman, D. Choudhury, and K. Ghosh, Search for exotic leptons in final states with two or three leptons and fat-jets at 13 TeV LHC, J. High Energy Phys. 04 (2022) 150.

[14] S. Ashanujjaman and K. Ghosh, Revisiting type-II seesaw: Present limits and future prospects at LHC, J. High Energy Phys. 03 (2022) 195.

[15] R. Foot, H. Lew, X. G. He, and G. C. Joshi, Seesaw neutrino masses induced by a triplet of leptons, Z. Phys. C **44**, 441 (1989).

[16] S. Ashanujjaman and K. Ghosh, Type-III see-saw: Search for triplet fermions in final states with multiple leptons and fat-jets at 13 TeV LHC, Phys. Lett. B **825**, 136889 (2022).

[17] S. Ashanujjaman and K. Ghosh, Type-III see-saw: Phenomenological implications of the information lost in decoupling from high-energy to low-energy, Phys. Lett. B **819**, 136403 (2021).

[18] E. Di Valentino, S. Gariazzo, and O. Mena, Most constraining cosmological neutrino mass bounds, Phys. Rev. D **104**, 083504 (2021).

[19] S. Jangid, P. Bandyopadhyay, P. S. Bhupal Dev, and A. Kumar, Vacuum stability in inert Higgs doublet model with right-handed neutrinos, J. High Energy Phys. 08 (2020) 154.

[20] S. Jangid and P. Bandyopadhyay, Distinguishing inert Higgs doublet and inert triplet scenarios, Eur. Phys. J. C **80**, 715 (2020).

[21] P. Bandyopadhyay, S. Jangid, and M. Mitra, Scrutinizing vacuum stability in IDM with type-III inverse seesaw, J. High Energy Phys. 02 (**2021**) 075.

[22] F. Bonnet, M. Hirsch, T. Ota, and W. Winter, Systematic study of the $d = 5$ Weinberg operator at one-loop order, J. High Energy Phys. 07 (**2012**) 153.

[23] E. Ma, Pathways to naturally small neutrino masses, Phys. Rev. Lett. **81**, 1171 (1998).

[24] K. S. Babu, Model of "Calculable" Majorana neutrino masses, Phys. Lett. B **203**, 132 (1988).

[25] P. Fileviez Perez and M. B. Wise, On the origin of neutrino masses, Phys. Rev. D **80**, 053006 (2009).

[26] K. S. Babu and C. Macesanu, Two loop neutrino mass generation and its experimental consequences, Phys. Rev. D **67**, 073010 (2003).

[27] L. M. Krauss, S. Nasri, and M. Trodden, A model for neutrino masses and dark matter, Phys. Rev. D **67**, 085002 (2003).

[28] K. Cheung and O. Seto, Phenomenology of TeV right-handed neutrino and the dark matter model, Phys. Rev. D **69**, 113009 (2004).

[29] E. Ma, Verifiable radiative seesaw mechanism of neutrino mass and dark matter, Phys. Rev. D **73**, 077301 (2006).

[30] E. Ma and U. Sarkar, Revelations of the E(6)/U(1)(N) model: Two-loop neutrino mass and dark matter, Phys. Lett. B **653**, 288 (2007).

[31] M. Aoki, S. Kanemura, and O. Seto, Neutrino Mass, Dark Matter and Baryon Asymmetry via TeV-Scale Physics without Fine-Tuning, Phys. Rev. Lett. **102**, 051805 (2009).

[32] M. Aoki, S. Kanemura, and O. Seto, A model of TeV scale physics for neutrino mass, dark matter and baryon asymmetry and its phenomenology, Phys. Rev. D **80**, 033007 (2009).

[33] D. Aristizabal Sierra and M. Hirsch, Experimental tests for the Babu-Zee two-loop model of Majorana neutrino masses, J. High Energy Phys. 12 (2006) 052.

[34] Avnish and K. Ghosh, Multi-charged TeV scale scalars and fermions in the framework of a radiative seesaw model, arXiv:2007.01766.

[35] F. Bonnet, D. Hernandez, T. Ota, and W. Winter, Neutrino masses from higher than $d = 5$ effective operators, J. High Energy Phys. 10 (2009) 076.

[36] S. Kanemura and T. Ota, Neutrino masses from loop-induced $d \geq 7$ operators, Phys. Lett. B **694**, 233 (2010).

[37] G. Anamiati, O. Castillo-Felisola, R. M. Fonseca, J. C. Helo, and M. Hirsch, High-dimensional neutrino masses, J. High Energy Phys. 12 (**2018**) 066.

[38] K. Kumericki, I. Picek, and B. Radovcic, TeV-scale seesaw with quintuplet fermions, Phys. Rev. D **86**, 013006 (2012).

[39] K. Kumericki, I. Picek, and B. Radovcic, Exotic seesaw-motivated heavy leptons at the LHC, Phys. Rev. D **84**, 093002 (2011).

[40] S. Ashanujjaman and K. Ghosh, A genuine fermionic quintuplet seesaw model: Phenomenological introduction, J. High Energy Phys. 06 (2021) 084.

[41] B. Abi *et al.* (Muon $g-2$ Collaboration), Measurement of the Positive Muon Anomalous Magnetic Moment to 0.46 ppm, Phys. Rev. Lett. **126**, 141801 (2021).

[42] G. W. Bennett *et al.* (Muon $g-2$ Collaboration), Final report of the muon E821 anomalous magnetic moment measurement at BNL, Phys. Rev. D **73**, 072003 (2006).

[43] T. Aoyama *et al.*, The anomalous magnetic moment of the muon in the Standard Model, Phys. Rep. **887**, 1 (2020).

[44] S. Borsanyi *et al.*, Leading hadronic contribution to the muon magnetic moment from lattice QCD, Nature (London) **593**, 51 (2021).

[45] T. Aoyama, M. Hayakawa, T. Kinoshita, and M. Nio, Complete Tenth-Order QED Contribution to the Muon $g-2$, Phys. Rev. Lett. **109**, 111808 (2012).

[46] A. Czarnecki, W. J. Marciano, and A. Vainshtein, Refinements in electroweak contributions to the muon anomalous magnetic moment, Phys. Rev. D **67**, 073006 (2003); **73**, 119901(E) (2006).

[47] C. Gnendiger, D. Stöckinger, and H. Stöckinger-Kim, The electroweak contributions to $(g-2)_\mu$ after the Higgs boson mass measurement, Phys. Rev. D **88**, 053005 (2013).

[48] M. Davier, A. Hoecker, B. Malaescu, and Z. Zhang, Reevaluation of the hadronic vacuum polarisation contributions to the Standard Model predictions of the muon $g-2$ and $\alpha(m_Z^2)$ using newest hadronic cross-section data, Eur. Phys. J. C **77**, 827 (2017).

[49] A. Keshavarzi, D. Nomura, and T. Teubner, Muon $g-2$ and $\alpha(M_Z^2)$: A new data-based analysis, Phys. Rev. D **97**, 114025 (2018).

[50] M. Hoferichter, B.-L. Hoid, B. Kubis, S. Leupold, and S. P. Schneider, Dispersion relation for hadronic light-by-light scattering: Pion pole, J. High Energy Phys. 10 (2018) 141.

[51] J. Bijnens, N. Hermansson-Truedsson, and A. Rodríguez-Sánchez, Short-distance constraints for the HLbL contribution to the muon anomalous magnetic moment, Phys. Lett. B **798**, 134994 (2019).

[52] G. Colangelo, F. Hagelstein, M. Hoferichter, L. Laub, and P. Stoffer, Longitudinal short-distance constraints for the hadronic light-by-light contribution to $(g-2)_\mu$ with large-N_c Regge models, J. High Energy Phys. 03 (2020) 101.

[53] R. H. Parker, C. Yu, W. Zhong, B. Estey, and H. Müller, Measurement of the fine-structure constant as a test of the Standard Model, Science **360**, 191 (2018).

[54] L. Morel, Z. Yao, P. Cladé, and S. Guellati-Khélifa, Determination of the fine-structure constant with an accuracy of 81 parts per trillion, Nature (London) **588**, 61 (2020).

[55] C. Biggio, The contribution of fermionic seesaws to the anomalous magnetic moment of leptons, Phys. Lett. B **668**, 378 (2008).

[56] S. Zhou, Neutrino masses, leptonic flavor mixing, and muon $(g-2)$ in the seesaw model with the gauge symmetry *, Chin. Phys. C **46**, 011001 (2022).

[57] I. Doršner, S. Fajfer, A. Greljo, J. F. Kamenik, and N. Košnik, Physics of leptoquarks in precision experiments and at particle colliders, Phys. Rep. **641**, 1 (2016).

[58] D. Aristizabal Sierra, M. Hirsch, and S. G. Kovalenko, Leptoquarks: Neutrino masses and accelerator phenomenology, Phys. Rev. D **77**, 055011 (2008).

[59] I. Doršner, S. Fajfer, and N. Košnik, Leptoquark mechanism of neutrino masses within the grand unification framework, Eur. Phys. J. C **77**, 417 (2017).

[60] K. S. Babu, P. S. B. Dev, S. Jana, and A. Thapa, Non-standard interactions in radiative neutrino mass models, J. High Energy Phys. 03 (2020) 006.

[61] H. Päs and E. Schumacher, Common origin of R_K and neutrino masses, Phys. Rev. D **92**, 114025 (2015).

[62] C.-K. Chua, X.-G. He, and W.-Y. P. Hwang, Neutrino mass induced radiatively by supersymmetric leptoquarks, Phys. Lett. B **479**, 224 (2000).

[63] U. Mahanta, Neutrino masses and mixing angles from leptoquark interactions, Phys. Rev. D **62**, 073009 (2000).

[64] K. S. Babu and J. Julio, Two-loop neutrino mass generation through leptoquarks, Nucl. Phys. **B841**, 130 (2010).

[65] D. Zhang, Radiative neutrino masses, lepton flavor mixing and muon $g-2$ in a leptoquark model, J. High Energy Phys. 07 (2021) 069.

[66] H. Georgi and S. L. Glashow, Unity of All Elementary Particle Forces, Phys. Rev. Lett. **32**, 438 (1974).

[67] H. Georgi, The state of the art—Gauge theories, AIP Conf. Proc. **23**, 575 (1975).

[68] H. Fritzsch and P. Minkowski, Unified interactions of leptons and hadrons, Ann. Phys. (N.Y.) **93**, 193 (1975).

[69] S. Dimopoulos and L. Susskind, Mass without scalars, Nucl. Phys. **B155**, 237 (1979).

[70] E. Farhi and L. Susskind, Technicolor, Phys. Rep. **74**, 277 (1981).

[71] B. Schrempp and F. Schrempp, Light leptoquarks, Phys. Lett. B **153**, 101 (1985).

[72] J. Wudka, Composite leptoquarks, Phys. Lett. B **167**, 337 (1986).

[73] H. P. Nilles, Supersymmetry, supergravity and particle physics, Phys. Rep. **110**, 1 (1984).

[74] H. E. Haber and G. L. Kane, The search for supersymmetry: Probing physics beyond the standard model, Phys. Rep. **117**, 75 (1985).

[75] N. Assad, B. Fornal, and B. Grinstein, Baryon number and lepton universality violation in leptoquark and diquark models, Phys. Lett. B **777**, 324 (2018).

[76] P. Fileviez Perez, C. Murgui, and A. D. Plascencia, Leptoquarks and matter unification: Flavor anomalies and the muon $g-2$, Phys. Rev. D **104**, 035041 (2021).

[77] C. Murgui and M. B. Wise, Scalar leptoquarks, baryon number violation, and Pati-Salam symmetry, Phys. Rev. D **104**, 035017 (2021).

[78] G. Couture and H. Konig, Bounds on second generation scalar leptoquarks from the anomalous magnetic moment of the muon, Phys. Rev. D **53**, 555 (1996).

[79] D. Marzocca, Addressing the B-physics anomalies in a fundamental composite Higgs model, J. High Energy Phys. 07 (2018) 121.

[80] V. Gherardi, D. Marzocca, and E. Venturini, Low-energy phenomenology of scalar leptoquarks at one-loop accuracy, J. High Energy Phys. 01 (2021) 138.

[81] A. Crivellin, D. Müller, and T. Ota, Simultaneous explanation of $R(D^{(*)})$ and $b \to s\mu^+\mu^-$: The last scalar leptoquarks standing, J. High Energy Phys. 09 (2017) 040.

[82] A. Crivellin, D. Müller, and F. Saturnino, Flavor phenomenology of the leptoquark singlet-triplet model, J. High Energy Phys. 06 (2020) 020.

[83] U. Aydemir, T. Mandal, and S. Mitra, Addressing the $\mathbf{R}_{D^{(*)}}$ anomalies with an $\mathbf{S}_1$ leptoquark from $\mathbf{SO(10)}$ grand unification, Phys. Rev. D **101**, 015011 (2020).

[84] D. Bečirević, I. Doršner, S. Fajfer, N. Košnik, D. A. Faroughy, and O. Sumensari, Scalar leptoquarks from grand unified theories to accommodate the B-physics anomalies, Phys. Rev. D **98**, 055003 (2018).

[85] I. Bigaran, J. Gargalionis, and R. R. Volkas, A near-minimal leptoquark model for reconciling flavour anomalies and generating radiative neutrino masses, J. High Energy Phys. 10 (2019) 106.

[86] T. Mandal, S. Mitra, and S. Raz, $R_{D^{(*)}}$ motivated $\mathcal{S}_1$ leptoquark scenarios: Impact of interference on the exclusion limits from LHC data, Phys. Rev. D **99**, 055028 (2019).

[87] S. Iguro, M. Takeuchi, and R. Watanabe, Testing leptoquark/EFT in $\bar{B} \to D^{(*)} l\bar{\nu}$ at the LHC, Eur. Phys. J. C **81**, 406 (2021).

[88] H. M. Lee, Leptoquark option for B-meson anomalies and leptonic signatures, Phys. Rev. D **104**, 015007 (2021).

[89] M. Bordone, O. Catà, T. Feldmann, and R. Mandal, Constraining flavour patterns of scalar leptoquarks in the effective field theory, J. High Energy Phys. 03 (2021) 122.

[90] I. Bigaran and R. R. Volkas, Reflecting on chirality: CP-violating extensions of the single scalar-leptoquark solutions for the $(g-2)\mathrm{e}, \mu$ puzzles and their implications for lepton EDMs, Phys. Rev. D **105**, 015002 (2022).

[91] C. Borschensky, B. Fuks, A. Kulesza, and D. Schwartländer, Scalar leptoquark pair production at the LHC: Precision predictions in the era of flavour anomalies, J. High Energy Phys. 02 (2022) 157.

[92] A. Dedes and K. Mantzaropoulos, Universal scalar leptoquark action for matching, J. High Energy Phys. 11 (2021) 166.

[93] T. E. Browder, N. G. Deshpande, R. Mandal, and R. Sinha, Impact of $B \to K\nu\nu$ measurements on beyond the Standard Model theories, Phys. Rev. D **104**, 053007 (2021).

[94] J.-H. Sheng, J. Zhu, and Q.-Y. Hu, Investigation on the new physics effects of the vector leptoquark on semileptonic $\bar{B}^* \to V\tau^-\overline{\nu_\tau}$ decays, Eur. Phys. J. C **81**, 524 (2021).

[95] C. Cornella, D. A. Faroughy, J. Fuentes-Martin, G. Isidori, and M. Neubert, Reading the footprints of the B-meson flavor anomalies, J. High Energy Phys. 08 (2021) 050.

[96] A. Crivellin, J. F. Eguren, and J. Virto, Next-to-leading-order QCD matching for $\Delta F = 2$ processes in scalar leptoquark models, J. High Energy Phys. 03 (2022) 185.

[97] A. Angelescu, D. Bečirević, D. A. Faroughy, F. Jaffredo, and O. Sumensari, Single leptoquark solutions to the B-physics anomalies, Phys. Rev. D **104**, 055017 (2021).

[98] A. Angelescu, D. Bečirević, D. A. Faroughy, and O. Sumensari, Closing the window on single leptoquark solutions to the B-physics anomalies, J. High Energy Phys. 10 (2018) 183.

[99] P. Arnan, D. Becirevic, F. Mescia, and O. Sumensari, Probing low energy scalar leptoquarks by the leptonic W and Z couplings, J. High Energy Phys. 02 (2019) 109.

[100] E. Coluccio Leskow, G. D'Ambrosio, A. Crivellin, and D. Müller, $(g-2)\mu$, lepton flavor violation, and Z decays with leptoquarks: Correlations and future prospects, Phys. Rev. D **95**, 055018 (2017).

[101] A. Crivellin, C. Greub, D. Müller, and F. Saturnino, Scalar leptoquarks in leptonic processes, J. High Energy Phys. 02 (2021) 182.

[102] A. Bhaskar, A. A. Madathil, T. Mandal, and S. Mitra, Combined explanation of W-mass, muon $g-2$, $R_{K^{(*)}}$ and $R_{D^{(*)}}$ anomalies in a singlet-triplet scalar leptoquark model, arXiv:2204.09031.

[103] N. Ghosh, S. K. Rai, and T. Samui, Collider signatures of a scalar leptoquark and vectorlike lepton in light of muon anomaly, arXiv:2206.11718.

[104] P. Bandyopadhyay and R. Mandal, Revisiting scalar leptoquark at the LHC, Eur. Phys. J. C **78**, 491 (2018).

[105] A. Bhaskar, T. Mandal, and S. Mitra, Boosting vector leptoquark searches with boosted tops, Phys. Rev. D **101**, 115015 (2020).

[106] A. Bhaskar, D. Das, T. Mandal, S. Mitra, and C. Neeraj, Precise limits on the charge-2/3 U1 vector leptoquark, Phys. Rev. D **104**, 035016 (2021).

[107] A. Bhaskar, T. Mandal, S. Mitra, and M. Sharma, Improving third-generation leptoquark searches with combined signals and boosted top quarks, Phys. Rev. D **104**, 075037 (2021).

[108] L. Da Rold, M. Epele, A. Medina, N. I. Mileo, and A. Szynkman, Enhancement of the double Higgs production via leptoquarks at the LHC, J. High Energy Phys. 08 (2021) 100.

[109] G. Hiller, D. Loose, and I. Nišandžić, Flavorful leptoquarks at the LHC and beyond: Spin 1, J. High Energy Phys. 06 (2021) 080.

[110] U. Haisch and G. Polesello, Resonant third-generation leptoquark signatures at the Large Hadron Collider, J. High Energy Phys. 05 (2021) 057.

[111] K. Chandak, T. Mandal, and S. Mitra, Hunting for scalar leptoquarks with boosted tops and light leptons, Phys. Rev. D **100**, 075019 (2019).

[112] A. Bhaskar, D. Das, B. De, and S. Mitra, Enhancing scalar productions with leptoquarks at the LHC, Phys. Rev. D **102**, 035002 (2020).

[113] A. Alves, O. J. P. t. Eboli, G. Grilli Di Cortona, and R. R. Moreira, Indirect and monojet constraints on scalar leptoquarks, Phys. Rev. D **99**, 095005 (2019).

[114] I. Doršner, S. Fajfer, and M. Patra, A comparative study of the S_1 and U_1 leptoquark effects in the light quark regime, Eur. Phys. J. C **80**, 204 (2020).

[115] S. Mandal, M. Mitra, and N. Sinha, Probing leptoquarks and heavy neutrinos at the LHeC, Phys. Rev. D **98**, 095004 (2018).

[116] R. Padhan, S. Mandal, M. Mitra, and N. Sinha, Signatures of $\tilde{R}_2$ class of leptoquarks at the upcoming ep colliders, Phys. Rev. D **101**, 075037 (2020).

[117] M. J. Baker, J. Fuentes-Martín, G. Isidori, and M. König, High- p_T signatures in vector-leptoquark models, Eur. Phys. J. C **79**, 334 (2019).

[118] H. Nadeau and D. London, Leptoquarks at e gamma colliders, Phys. Rev. D **47**, 3742 (1993).

[119] S. Atag and O. Cakir, Pair production of scalar leptoquarks at TeV energy gamma p colliders, Phys. Rev. D **49**, 5769 (1994).

[120] S. Atag, A. Celikel, and S. Sultansoy, Scalar leptoquark production at TeV energy gamma p colliders, Phys. Lett. B **326**, 185 (1994).

[121] W. Buchmuller, R. Ruckl, and D. Wyler, Leptoquarks in lepton-quark collisions, Phys. Lett. B **191**, 442 (1987); **448**, 320(E) (1999).

[122] J. L. Hewett and S. Pakvasa, Leptoquark production in hadron colliders, Phys. Rev. D **37**, 3165 (1988).

[123] J. L. Hewett and T. G. Rizzo, Leptoquark signals at $e^+ e^-$ colliders, Phys. Rev. D **36**, 3367 (1987).

[124] F. Cuypers, Leptoquark production in e—gamma scattering, Nucl. Phys. **B474**, 57 (1996).

[125] J. Blumlein, E. Boos, and A. Kryukov, Leptoquark pair production in hadronic interactions, Z. Phys. C **76**, 137 (1997).

[126] A. Belyaev, C. Leroy, R. Mehdiyev, and A. Pukhov, Leptoquark single and pair production at LHC with CalcHEP/CompHEP in the complete model, J. High Energy Phys. 09 (2005) 005.

[127] M. Kramer, T. Plehn, M. Spira, and P. M. Zerwas, Pair production of scalar leptoquarks at the tevatron, Phys. Rev. Lett. **79**, 341 (1997).

[128] T. Plehn, H. Spiesberger, M. Spira, and P. M. Zerwas, Formation and decay of scalar leptoquarks/squarks in e p collisions, Z. Phys. C **74**, 611 (1997).

[129] O. J. P. Eboli, R. Zukanovich Funchal, and T. L. Lungov, Signal and backgrounds for leptoquarks at the CERN LHC, Phys. Rev. D **57**, 1715 (1998).

[130] M. Kramer, T. Plehn, M. Spira, and P. M. Zerwas, Pair production of scalar leptoquarks at the CERN LHC, Phys. Rev. D **71**, 057503 (2005).
[131] J. B. Hammett and D. A. Ross, NLO leptoquark production and decay: The narrow-width approximation and beyond, J. High Energy Phys. 07 (2015) 148.
[132] T. Mandal, S. Mitra, and S. Seth, Single productions of colored particles at the LHC: An example with scalar leptoquarks, J. High Energy Phys. 07 (2015) 028.
[133] P. Asadi, R. Capdevilla, C. Cesarotti, and S. Homiller, Searching for leptoquarks at future muon colliders, J. High Energy Phys. 10 (2021) 182.
[134] P. Bandyopadhyay, A. Karan, R. Mandal, and S. Parashar, Distinguishing signatures of scalar leptoquarks at hadron and muon colliders, Eur. Phys. J. C **82**, 916 (2022).
[135] S. Davidson, D. C. Bailey, and B. A. Campbell, Model independent constraints on leptoquarks from rare processes, Z. Phys. C **61**, 613 (1994).
[136] R. Mandal and A. Pich, Constraints on scalar leptoquarks from lepton and kaon physics, J. High Energy Phys. 12 (2019) 089.
[137] U. K. Dey, D. Kar, M. Mitra, M. Spannowsky, and A. C. Vincent, Searching for leptoquarks at IceCube and the LHC, Phys. Rev. D **98**, 035014 (2018).
[138] A. Crivellin, D. Müller, and L. Schnell, Combined constraints on first generation leptoquarks, Phys. Rev. D **103**, 115023 (2021).
[139] K. Kowalska, E. M. Sessolo, and Y. Yamamoto, Constraints on charmphilic solutions to the muon $g-2$ with leptoquarks, Phys. Rev. D **99**, 055007 (2019).
[140] H. J. Behrend *et al.* (CELLO Collaboration), Search for light leptoquark bosons, Phys. Lett. B **178**, 452 (1986); **184**, 417(A) (1987).
[141] W. Bartel *et al.* (JADE Collaboration), Search for leptoquarks and other new particles with lepton-hadron signature in e^+e^- interactions, Z. Phys. C **36**, 15 (1987).
[142] G. N. Kim *et al.* (AMY Collaboration), A search for leptoquark and colored lepton pair production in e^+e^- annihilations at TRISTAN, Phys. Lett. B **240**, 243 (1990).
[143] P. Abreu *et al.* (DELPHI Collaboration), Search for leptoquarks and FCNC in e^+e^- annihilations at $S^{(1/2)} = 183$-GeV, Phys. Lett. B **446**, 62 (1999).
[144] F. D. Aaron *et al.* (H1 Collaboration), Search for first generation leptoquarks in ep collisions at HERA, Phys. Lett. B **704**, 388 (2011).
[145] H. Abramowicz *et al.* (ZEUS Collaboration), Limits on contact interactions and leptoquarks at HERA, Phys. Rev. D **99**, 092006 (2019).
[146] J. Alitti *et al.* (UA2 Collaboration), A search for scalar leptoquarks at the CERN anti-p p collider, Phys. Lett. B **274**, 507 (1992).
[147] V. M. Abazov *et al.* (D0 Collaboration), Search for first generation leptoquark pair production in the electron + missing energy + jets final state, Phys. Rev. D **84**, 071104 (2011).
[148] T. Aaltonen *et al.* (CDF Collaboration), Search for third generation vector leptoquarks in $p\bar{p}$ collisions at $\sqrt{s} = 1.96$-TeV, Phys. Rev. D **77**, 091105 (2008).
[149] G. Aad *et al.* (ATLAS Collaboration), Search for pairs of scalar leptoquarks decaying into quarks and electrons or muons in $\sqrt{s} = 13$ TeV pp collisions with the ATLAS detector, J. High Energy Phys. 10 (2020) 112.
[150] CMS Collaboration, Search for singly and pair-produced leptoquarks coupling to third-generation fermions in proton-proton collisions at $\sqrt{s} = 13$ TeV, Phys. Lett. B **819**, 136446 (2021).
[151] G. Aad *et al.* (ATLAS Collaboration), Search for pair production of third-generation scalar leptoquarks decaying into a top quark and a τ-lepton in pp collisions at $\sqrt{s} = 13$ TeV with the ATLAS detector, J. High Energy Phys. 06 (2021) 179.
[152] A. M. Sirunyan *et al.* (CMS Collaboration), Constraints on models of scalar and vector leptoquarks decaying to a quark and a neutrino at $\sqrt{s} = 13$ TeV, Phys. Rev. D **98**, 032005 (2018).
[153] A. M. Sirunyan *et al.* (CMS Collaboration), Search for singly and pair-produced leptoquarks coupling to third-generation fermions in proton-proton collisions at $s = 13$ TeV, Phys. Lett. B **819**, 136446 (2021).
[154] P. Bandyopadhyay, S. Dutta, and A. Karan, Investigating the production of leptoquarks by means of zeros of amplitude at photon electron collider, Eur. Phys. J. C **80**, 573 (2020).
[155] P. Bandyopadhyay, S. Dutta, and A. Karan, Zeros of amplitude in the associated production of photon and leptoquark at $e-p$ collider, Eur. Phys. J. C **81**, 315 (2021).
[156] P. Bandyopadhyay, S. Dutta, M. Jakkapu, and A. Karan, Distinguishing leptoquarks at the LHC/FCC, Nucl. Phys. **B971**, 115524 (2021).
[157] S. Dutta, P. Bandyopadhyay, and A. Karan, Distinguishing different BSM signatures at present and future colliders, arXiv:2105.00893.
[158] P. Bandyopadhyay and R. Mandal, Vacuum stability in an extended standard model with a leptoquark, Phys. Rev. D **95**, 035007 (2017).
[159] P. Bandyopadhyay, S. Jangid, and A. Karan, Constraining scalar doublet and triplet leptoquarks with vacuum stability and perturbativity, Eur. Phys. J. C **82**, 516 (2022).
[160] F. F. Freitas, J. a. Gonçalves, A. P. Morais, R. Pasechnik, and W. Porod, On interplay between flavour anomalies and neutrino properties, arXiv:2206.01674.
[161] R. Coy and M. Frigerio, Effective comparison of neutrino-mass models, Phys. Rev. D **105**, 115041 (2022).
[162] O. Catà and T. Mannel, Linking lepton number violation with B anomalies, arXiv:1903.01799.
[163] S.-L. Chen, W.-w. Jiang, and Z.-K. Liu, Combined explanations of B-physics anomalies, $(g-2)_{e,\mu}$ and neutrino masses by scalar leptoquarks, Eur. Phys. J. C **82**, 959 (2022).
[164] P. Azzi *et al.*, Report from Working Group 1: Standard Model physics at the HL-LHC and HE-LHC, CERN Yellow Rep. Monogr. **7**, 1 (2019).
[165] M. Cepeda *et al.*, Report from Working Group 2: Higgs physics at the HL-LHC and HE-LHC, CERN Yellow Rep. Monogr. **7**, 221 (2019).
[166] A. Abada *et al.* (FCC Collaboration), FCC physics opportunities: Future circular collider conceptual design report volume 1, Eur. Phys. J. C **79**, 474 (2019).
[167] I. Dorsner, S. Fajfer, and N. Kosnik, Heavy and light scalar leptoquarks in proton decay, Phys. Rev. D **86**, 015013 (2012).

[168] F. Staub, Exploring new models in all detail with SARAH, Adv. High Energy Phys. **2015**, 840780 (2015).
[169] W. Porod, SPheno, A program for calculating supersymmetric spectra, SUSY particle decays and SUSY particle production at e+ e- colliders, Comput. Phys. Commun. **153**, 275 (2003).
[170] W. Porod and F. Staub, SPheno 3.1: Extensions including flavour, *CP* phases and models beyond the MSSM, Comput. Phys. Commun. **183**, 2458 (2012).
[171] J. Alwall, M. Herquet, F. Maltoni, O. Mattelaer, and T. Stelzer, Madgraph 5: Going beyond, J. High Energy Phys. 06 (2011) 128.
[172] A. M. Sirunyan *et al.* (CMS Collaboration), Search for pair production of first-generation scalar leptoquarks at $\sqrt{s} = 13$ TeV, Phys. Rev. D **99**, 052002 (2019).
[173] A. M. Sirunyan *et al.* (CMS Collaboration), Search for pair production of second-generation leptoquarks at $\sqrt{s} = 13$ TeV, Phys. Rev. D **99**, 032014 (2019).
[174] G. Aad *et al.* (ATLAS Collaboration), Search for pairs of scalar leptoquarks decaying into quarks and electrons or muons in $\sqrt{s} = 13$ TeV pp collisions with the ATLAS detector, J. High Energy Phys. 10 (2020) 112.
[175] T. Aaltonen *et al.* (CDF Collaboration), High-precision measurement of the W boson mass with the CDF II detector, Science **376**, 170 (2022).
[176] P. F. de Salas, D. V. Forero, S. Gariazzo, P. Martínez-Miravé, O. Mena, C. A. Ternes, M. Tórtola, and J. W. F. Valle, 2020 global reassessment of the neutrino oscillation picture, J. High Energy Phys. 02 (2021) 071.
[177] A. M. Baldini *et al.* (MEG Collaboration), Search for the lepton flavour violating decay $\mu^+ \to e^+\gamma$ with the full dataset of the MEG experiment, Eur. Phys. J. C **76**, 434 (2016).
[178] W. H. Bertl *et al.* (SINDRUM II Collaboration), A search for muon to electron conversion in muonic gold, Eur. Phys. J. C **47**, 337 (2006).
[179] A. Belyaev, N. D. Christensen, and A. Pukhov, CalcHEP 3.4 for collider physics within and beyond the Standard Model, Comput. Phys. Commun. **184**, 1729 (2013).
[180] T. Sjöstrand, S. Ask, J. R. Christiansen, R. Corke, N. Desai, P. Ilten, S. Mrenna, S. Prestel, C. O. Rasmussen, and P. Z. Skands, An introduction to PYTHIA 8.2, Comput. Phys. Commun. **191**, 159 (2015).
[181] M. Cacciari, G. P. Salam, and G. Soyez, FASTJET User Manual, Eur. Phys. J. C **72**, 1896 (2012).
[182] CMS Collaboration, A Cambridge-Aachen (C-A) based jet algorithm for boosted top-jet tagging, Report No. CMS-PAS-JME-09-001.
[183] A. M. Sirunyan *et al.* (CMS Collaboration), Identification of heavy-flavour jets with the CMS detector in pp collisions at 13 TeV, J. Instrum. **13**, P05011 (2018).
[184] E. Bols, J. Kieseler, M. Verzetti, M. Stoye, and A. Stakia, Jet flavour classification using DEEPJET, J. Instrum. **15**, P12012 (2020).
[185] A. M. Sirunyan *et al.* (CMS Collaboration), Performance of reconstruction and identification of τ leptons decaying to hadrons and ν_τ in pp collisions at $\sqrt{s} = 13$ TeV, J. Instrum. **13**, P10005 (2018).
[186] J. Pumplin, D. R. Stump, J. Huston, H. L. Lai, P. M. Nadolsky, and W. K. Tung, New generation of parton distributions with uncertainties from global QCD analysis, J. High Energy Phys. 07 (2002) 012.
[187] T. Mandal, S. Mitra, and S. Seth, Pair production of scalar leptoquarks at the LHC to NLO parton shower accuracy, Phys. Rev. D **93**, 035018 (2016).
[188] C. Borschensky, B. Fuks, A. Kulesza, and D. Schwartländer, Scalar leptoquark pair production at hadron colliders, Phys. Rev. D **101**, 115017 (2020).
[189] S. Fartoukh, S. Kostoglou, M. Solfaroli Camillocci, G. Arduini, H. Bartosik, C. Bracco *et al.*, LHC configuration and operational scenario for run 3, Technical Report No. CERN-ACC-2021-0007, CERN, Geneva, 2021.
[190] D. Krohn, M. D. Schwartz, T. Lin, and W. J. Waalewijn, Jet Charge at the LHC, Phys. Rev. Lett. **110**, 212001 (2013).
[191] A. M. Sirunyan *et al.* (CMS Collaboration), Measurements of jet charge with dijet events in pp collisions at $\sqrt{s} = 8$ TeV, J. High Energy Phys. 10 (2017) 131.
[192] S. Tokar (ATLAS, CMS Collaborations), Jet charge determination at the LHC, in *Proceedings of parton radiation and fragmentation from LHC to FCC-ee* (2017), 2, pp. 79–84.
[193] V. Khachatryan *et al.* (CMS Collaboration), Jet energy scale and resolution in the CMS experiment in pp collisions at 8 TeV, J. Instrum. **12**, P02014 (2017).
[194] A. M. Sirunyan *et al.* (CMS Collaboration), Performance of the reconstruction and identification of high-momentum muons in proton-proton collisions at $\sqrt{s} = 13$ TeV, J. Instrum. **15**, P02027 (2020).
[195] A. Tumasyan *et al.* (CMS Collaboration), Measurement of the top quark mass using events with a single reconstructed top quark in pp collisions at $\sqrt{s} = 13$ TeV, J. High Energy Phys. 12 (2021) 161.
[196] A. M. Sirunyan *et al.* (CMS Collaboration), A measurement of the Higgs boson mass in the diphoton decay channel, Phys. Lett. B **805**, 135425 (2020).
[197] A. M. Sirunyan *et al.* (CMS Collaboration), Measurements of properties of the Higgs boson decaying into the four-lepton final state in pp collisions at $\sqrt{s} = 13$ TeV, J. High Energy Phys. 11 (2017) 047.

Correction: The terms in the last paragraph of Sec. II, sixth complete sentence following Eq. (2.1), were incorrect and have been set right.